

**TERC PROJECT No. H-99: Modeling Secondary Organic Aerosol from Isoprene**

Submitted to

The Texas Environmental Research Consortium/Houston Advanced Research Center

by

Carolyn Jordan

Robert Griffin (Principal Investigator)<sup>a</sup>

The University of New Hampshire

Institute for the Study of Earth, Oceans, and Space

8 College Road

Durham, NH 03824

<sup>a</sup>Rice University

Department of Civil and Environmental Engineering

6100 Main Street, MS-318

Houston, TX 77005

DRAFT: December 11, 2009

## TABLE OF CONTENTS

Abstract	ii
Introduction	1
Approach and Model Description	3
Model Modifications	6
Results	11
Conclusions	47
References Cited	49

## **Abstract**

Although the yield for the formation of secondary organic aerosol (SOA) from the oxidation of isoprene is small relative to other compounds, it is important to understand this phenomenon because of the predominance of isoprene emissions on local, regional, and global scales. To that end, a zero-dimensional model that describes the gas-phase chemistry of isoprene and its daughter products and the thermodynamic phase partitioning of those products with low enough volatility to produce SOA has been developed. The gas-phase chemistry was developed in the framework of the Caltech Atmospheric Chemistry Mechanism, and the phase distribution was determined using a simplified version of the Model to Predict the Multi-phase Partitioning of Organics. Four scenarios were considered: a low-nitrogen oxide ( $\text{NO}_x$ ) photochemical scenario, a high- $\text{NO}_x$  photochemical scenario, a nitrate radical ( $\text{NO}_3$ ) scenario, and a scenario in which the small dicarbonyls glyoxal (GLY) and methyl glyoxal (MGLY) were taken up assuming first-order rate constants determined from the literature. Regardless of scenario, it appears that the most important routes for SOA formation come from the phase partitioning of non-volatile products (likely dimers, trimers, etc.). However, the most important route of formation of these non-volatile products depended strongly on the scenario. In the low- $\text{NO}_x$  case, oxidation of methacrolein (MCR) and epoxide products leads to these species. In the high- $\text{NO}_x$  case, the MCR case was most dominant (because epoxides are less likely to form in the presence of  $\text{NO}_x$ ). In the  $\text{NO}_3$  case, organic peroxy radical self reactions formed the non-volatile SOA products. It is hypothesized that the MCR-  $\text{NO}_3$  reaction also is important. For the simulation conditions chosen, the reactive uptake of GLY and MGLY is relatively less important than the formation of SOA from

thermodynamic partitioning of the non-volatile products.

## **Introduction**

Particulate matter (also known as aerosol) in the atmosphere affects climate (by absorbing outgoing longwave planetary radiation, scattering solar radiation, and/or influencing cloud properties and lifetime), human health, visibility by causing light extinction, heterogeneous chemistry, and transport/cycling of material (Seinfeld and Pandis, 2006). A significant fraction of atmospheric aerosol has been measured to be organic in nature. Organic aerosol (OA) can be primary OA (POA), meaning that it was emitted directly to the atmosphere from its source (including combustion, wave crashing, etc.). Depending on source, these particles may be fine or coarse, with the distinction between the two usually made at 2.5 micron in diameter. In contrast, secondary OA (SOA) is formed via the gas-particle partitioning of the oxidation products of volatile organic compounds (VOCs); SOA is believed generally to reside in the fine aerosol mode (Seinfeld and Pandis, 2006). Based on aerosol mass spectrometric measurements, it is believed that the bulk of the OA in the troposphere of the northern mid-latitudes is SOA (Zhang et al., 2007).

Despite hundreds of studies investigating the emission rates of POA and the formation processes and yields of SOA (Seinfeld and Pankow, 2003; Hallquist et al., 2009), three-dimensional air quality models traditionally have underestimated observed OA levels (Volkamer et al., 2006). Therefore, it is difficult to use such models for regulatory purposes with respect to OA. It is generally believed that this overall underprediction results from an underprediction of SOA formation. This could result from ignorance of certain SOA precursors (Goldstein and Galbally, 2007), ignorance of specific SOA-

forming processes (e.g., cloud processing, heterogeneous reactions, etc.) (Hallquist et al., 2009), or a combination thereof.

On a global scale, isoprene is the dominant VOC emitted, with emissions of approximately 500 TgC yr<sup>-1</sup> (Guenther et al., 1995); its emissions also are significant on local scales, including in southeast Texas (Wiedinmyer et al., 2001). Historically, it was believed that oxidation of isoprene by species such as the hydroxyl radical (OH), ozone (O<sub>3</sub>), and the nitrate radical (NO<sub>3</sub>) did not lead to SOA based on chamber experiments performed at elevated temperatures (Pandis et al., 1991). More recent evidence indicates that at more realistic temperatures, isoprene oxidation does lead to SOA formation; this evidence is based on both ambient measurements and chamber experiments (Claeys et al., 2004; Carlton et al., 2009). It is believed that the formation of SOA from isoprene can occur via several mechanisms. First, products whose concentrations exceed saturation will partition to the aerosol phase based on traditional thermodynamics (Raoult's Law) (Kroll et al., 2005a; Kroll et al., 2006; Ng et al., 2008). Second, aerosol uptake and subsequent aging (i.e., oligomerization) of small dicarbonyls (e.g., glyoxal (GLY) and methyl glyoxal (MGLY)) will increase particulate SOA mass (Kroll et al., 2005b; Fu et al., 2008). Finally, aqueous-phase (including cloud) processing of isoprene itself and its oxidation products can lead to residual SOA upon evaporation of the cloud droplet (Altieri et al., 2006; Carlton et al., 2006).

In this project, a mechanistic approach for simulation of SOA will be adopted using existing computer codes (the Caltech Atmospheric Chemistry Mechanism (CACM) and

the Model to Predict the Multi-phase Partitioning of Organics (MPMPO)) (Griffin et al., 2002; Griffin et al., 2003). These modules and the theory behind their development are described subsequently. Modifications to CACM and MPMPO will be made so that SOA formation from isoprene is described adequately by considering the first two pathways described above (traditional thermodynamics and reactive uptake). Cloud processing is not within the scope of this project. Originally, these modules were to have been implemented within a three-dimensional air quality model and applied to southeast Texas to simulate SOA formation in Houston, allowing for a comparison to data collected during the Texas Air Quality Study II (summer 2006). However, with the departure of Professor Daewon Byun from the University of Houston and with the publication of an important new paper describing gas-phase isoprene chemistry and its potential impact on subsequent SOA formation (Paulot et al., 2009), the focus of this project was changed to consider only zero-dimensional modeling.

### **Approach and Model Description**

In CACM, hundreds of VOCs are lumped according to source (biogenic versus anthropogenic), chemical structure, reactivity, and experimentally observed SOA formation potential. For example, lumped groups in CACM include OLEL (small carbon number alkenes), AROL (aromatic compounds with small SOA yields), and ALD2 (n-aldehydes with carbon numbers larger than two). Based on these same parameters and the prevalence of certain species (based on carbon number, isomeric form, etc.) within emission inventories in typical urban areas, surrogate structures are then assigned to the lumped VOC categories. For example, in CACM, 1-pentene is used as a surrogate for

OLEL, 1,2,3-trimethylbenzene is used as a surrogate for AROL, and n-pentaldehyde is used as a surrogate for ALD2. However, in certain cases, individual specific chemical species are tracked (as opposed to being assigned a lumped surrogate) within CACM based on uniqueness of emissions profiles or chemistry. Individual compounds tracked within CACM include methane, formaldehyde, acetaldehyde, and isoprene. CACM then predicts numerically the formation of multi-functional products that are created from the atmospheric oxidation of each of these surrogates or individual compounds by species including OH, NO<sub>3</sub>, and/or O<sub>3</sub>. This chemistry is predicted based on experimental studies from the literature, analogy to compounds with similar structures, or a published protocol for prediction of VOC oxidation chemistry (Jenkin et al., 1997). Detailed descriptions of the development and subsequent modifications/refinements to CACM are available in Griffin et al. (2002, 2005), Chen and Griffin (2005), Chen et al. (2006), and Jordan et al. (2008). In this project, the chemistry of isoprene within the CACM module will be updated. Again, the CACM module simulates only gas-phase chemistry.

Based on chemical structure (carbon number; number and type of functional groups such as alcohols, ketones, aldehydes, and carboxylic acids), products predicted by CACM are separated into two groups: those that are capable of partitioning to the aerosol phase and those that are not. This is essentially a separation based on expected vapor pressure. Note that this does not consider the second two pathways of SOA formation (reactive uptake and cloud processing) described above. Those products predicted by CACM that are deemed to have the potential to partition to SOA based on Raoult's Law are lumped according to source (biogenic versus anthropogenic), carbon number, volatility (as

predicted using a structure-activity approach), and dissociative capability within an aqueous phase (i.e., presence of at least one carboxylic acid structural moiety). As in the treatment of hundreds of VOCs using surrogates in CACM, these oxidation products are lumped into 14 surrogates that are used in partitioning calculations. For these 14 surrogates, a highly coupled, non-linear set of simultaneous equations can be written to describe equilibrium partitioning of each of these species between the gas phase and a condensed organic phase (Raoult's Law), equilibrium partitioning of each of these species between the gas phase and a condensed aqueous phase (Henry's Law), equilibrium between molecular and ionic forms of the species in the aqueous phase if applicable (dissociation), and a mass balance. Assuming that properties (vapor pressure, Henry's Law constant, activity coefficients in each condensed mixture, and dissociation constants) for each species are known or can be estimated using structure activity relationships, these equations are solved iteratively within the MPMPO module to predict the distribution of these compounds between the gas and condensed phases, with that residing in the condensed phase creating SOA. Detailed descriptions of the development and subsequent modifications/refinements to MPMPO are available in Pun et al. (2002), Griffin et al. (2003, 2005), Chen and Griffin (2005), Chen et al. (2006), and Jordan et al. (2008). Again, MPMPO must be used in conjunction with CACM to predict the phase distribution of products simulated by CACM. In this project, the updated chemistry of isoprene within CACM described above will be linked to MPMPO.

## Model Modifications

### CACM

Because necessary changes to MPMPO depend inextricably on changes made to the isoprene chemistry within CACM, requisite changes to CACM are described first. However, to understand why such changes are necessary, it is important to describe the treatment of isoprene within CACM prior to this project. The overall treatment of isoprene in the previously existing version of CACM is shown in Figure 1, which is taken directly from Griffin et al. (2002).

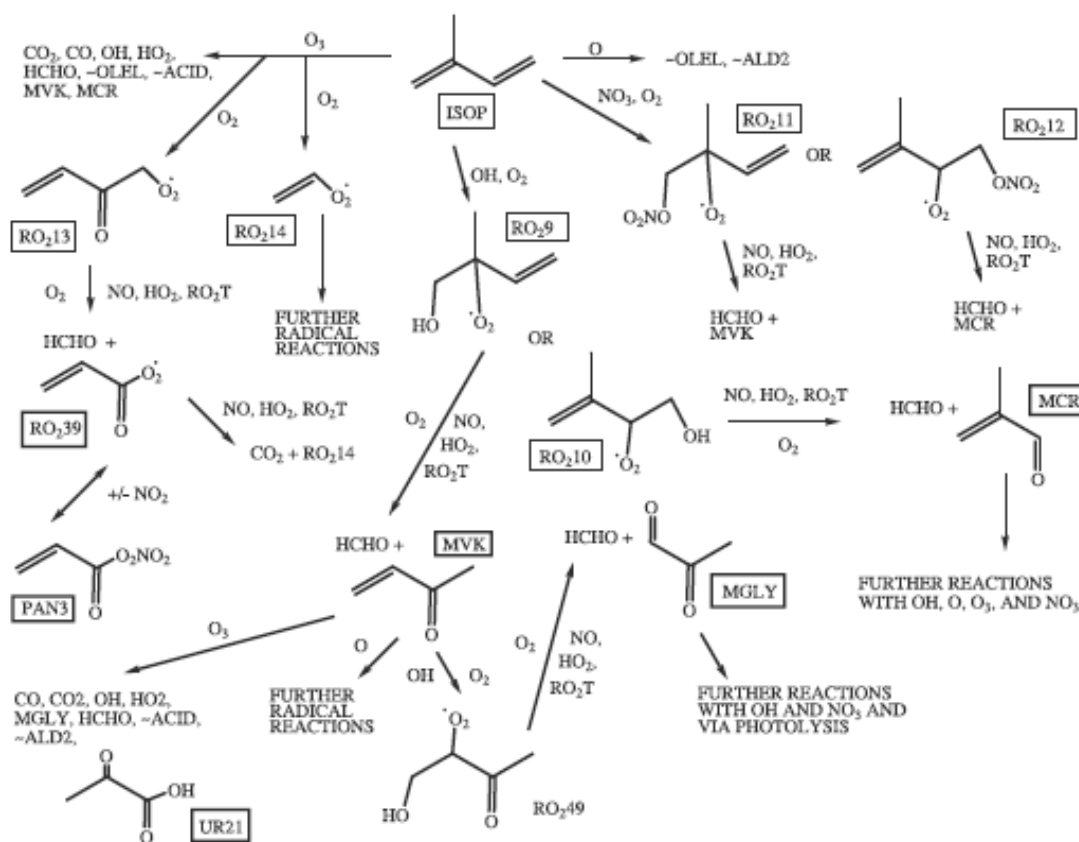


Figure 1. Isoprene (shown here as ISOP) chemistry within CACM as described by Griffin et al. (2002). This scheme served as the starting point for the work performed in the current project.

Figure 1 indicates that the oxidation of isoprene via multiple peroxy radical (RO<sub>2</sub>xx)

routes leads to stable products that include methacrolein (MCR), methyl vinyl ketone (MVK), MGLY, and keto-propanoic (pyruvic) acid (UR21) in CACM. In CACM, further reactions of MGLY can lead to (among other products) formation of UR21. Predicted concentrations of UR21 from this chemistry are small. When linked to MPMPO, UR21 is allowed to partition to the condensed phase, but its overall contribution to SOA formation is generally small. Other products are not included in the partitioning calculations, and as stated previously, the reactive uptake pathway for SOA formation for the small dicarbonyls and other products are not included in the previous version of the coupled CACM/MPMPO.

The gas-phase isoprene update involved changes to the further reactions of MCR as well as RO<sub>2</sub>-hydroperoxy radical (HO<sub>2</sub>) reaction sequences and RO<sub>2</sub>-RO<sub>2</sub> reaction sequences subsequent to OH-initiated oxidation of isoprene. In addition, the NO<sub>3</sub>-initiated reaction sequence was updated (principally the subsequent RO<sub>2</sub>-RO<sub>2</sub> reactions). Because the final code describing these reactions will be provided upon final quality checks (including commenting), only an overview will be provided here. It should be noted that no changes were made to MVK-associated chemistry because it is not believed to participate in SOA formation (Carlton et al., 2009).

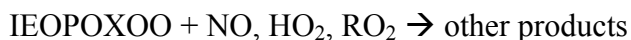
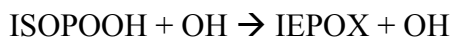
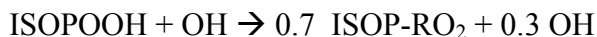
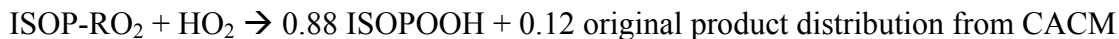
First, MCR appears to be a key intermediate in the formation of SOA from oxidation of isoprene, but the exact mechanism of this transformation remains unknown. Therefore, in order to account for this, the reaction in which MCR is oxidized by OH forms a non-volatile SOA product (NV), the stoichiometric coefficient of which was adjusted during

the modifications to MPMPO discussed below. This coefficient will be constrained between zero and unity, with the balance of the reaction forming the products considered in the previously existing version of the model. For the sake of the zero-dimensional modeling individual NV species will be tracked, but in potential future three-dimensional applications, these species could be lumped if needed.

The reactions of the major peroxy radicals formed from OH oxidation of isoprene with HO<sub>2</sub> have been updated substantially based on the recent paper by Paulot et al. (2009). Here, these peroxy radicals are assumed to form the corresponding hydroperoxide (ISOPOOH) at a yield of 0.88, with the balance going to OH, formaldehyde, and either MVK or MCR depending on which radical is reacting. Two pathways exist for ISOPOOH upon reaction with OH: formation of the corresponding isoprene epoxide (IEPOX) or reformation of the corresponding RO<sub>2</sub> and a hydroxycarbonyl. As with MCR, it is believed that IEPOX oxidation leads to SOA formation, but this mechanism is also unknown. Therefore, a similar approach is taken in which some fraction of IEPOX forms NV upon oxidation, while the balance forms a corresponding peroxy radical (IEPOXOO). This branching ratio was determined based on MPMPO updates discussed below. IEPOXOO reacts in a manner similar to other RO<sub>2</sub> to form products that include hydroxyacetone, glycoaldehyde, GLY, MGLY, formaldehyde, and formic acid. For RO<sub>2</sub>-RO<sub>2</sub> reactions, the only change is that a fraction of the reaction product is assumed to be NV based on formation of organic peroxides with large carbon numbers. The balance of the product distribution is that from the original CACM. Again, determination of this branching ratio was performed as part of the revisions to MPMPO.

The distribution (stoichiometric) of the isomers of the peroxy radicals from the NO<sub>3</sub>-initiated oxidation of isoprene (ISOP-NRO<sub>2</sub>) has been altered based on the recent work of Perring et al. (2009). This includes forming a new radical representing the δ configuration (and decreasing the stoichiometric yields of those that already existed in CACM). The reactions of the original peroxy radicals (which generally go to products that include MCR and MVK) remain unchanged. The δ-ISOP-NRO<sub>2</sub>, however, react with other RO<sub>2</sub> in a series of reactions that eventually form an organic peroxide product (ROOR) expected to partition to SOA.

A summary (greatly simplified) of significant modifications to CACM follows:



Again, the NV products are tracked individually, and the appropriate values of the stoichiometric coefficients ( $\alpha$ ,  $\beta$ , and  $\chi$ ) were determined during modification of MPMPO. Products expected to contribute to SOA include ISOPOOH, IEPOX, the series

of NV species, and ROOR.

### *MPMPO*

Because the chamber studies being simulated in this work included no aqueous solutions of inorganic aerosol and no POA (for the most part), an ideal solution can be assumed for the SOA, greatly simplifying necessary calculations within MPMPO because activity coefficients can be assumed to be unity (Seinfeld et al., 2001). The equations in MPMPO reduce to

$$K_i = \frac{A_i}{M_o G_i} \quad (1)$$

$$K_i = \frac{RT}{MW_i P_i^o} \quad (2)$$

$$M_o = \sum_i A_i \quad (3)$$

$$C_i = A_i + G_i \quad (4)$$

where  $K_i$  is the partitioning coefficient that describes the phase distribution of species  $i$ ,  $A_i$  is its aerosol-phase concentration,  $G_i$  is its gas-phase concentration,  $C_i$  is its total concentration (predicted by CACM),  $M_o$  is the total organic aerosol present (in this case equal to SOA),  $R$  is the ideal gas constant,  $T$  is temperature,  $MW_i$  is the molecular weight of species  $i$ , and  $P_i^o$  is the sub-cooled liquid vapor pressure of species  $i$  at  $T$ . If the molecular weight and vapor pressure of each partitioning species are known or can be predicted, equations (1) through (4) represent a series of equations that can be reduced to one equation that allows for the solution of  $M_o$ . This information was needed for ISOPOOH, IEPOX, ROOR, and the NV species. The properties of these compounds were assigned by analogy or by calculating their properties using structure-activity

relationships as described by Pun et al. (2002), Griffin et al. (2003, 2005), Chen and Griffin (2005), Chen et al. (2006), and Jordan et al. (2008). Simulations of chamber experiments were then performed using the updated simplified MPMPO module. The values of  $\alpha$ ,  $\beta$ , and  $\chi$  from the mechanistic summary above were used as fitting parameters in order to develop yields similar to those in Kroll et al. (2006) and Ng et al. (2008). These values are discussed in the SOA simulation section below.

The chamber experiments that were used to simulate the process above had no aqueous phase, which is believed to be necessary for the reactive uptake of GLY and MGLY. Therefore, this process was not considered in the above model development that was driven at understanding traditional organic solution thermodynamics (and to derive parameters such as  $\alpha$ ,  $\beta$ , and  $\chi$ ). However, in an effort to estimate how important this reactive uptake pathway could be on a relative scale, once the basic CACM and MPMPO approach was updated as discussed, loss of GLY and MGLY through reactive uptake was considered. For this effort, this loss was treated as a gas-phase reaction leading to NV:



The pseudo-first order reaction rate constants for this process were estimated from Fu et al. (2008) and are assumed to be  $0.049 \text{ hr}^{-1}$  and  $0.073 \text{ hr}^{-1}$  for GLY and MGLY, respectively.

## **Results**

### *CACM*

Because gas-phase simulations were performed during the original development of

CACM to test the overall ability of the model to simulate major species such as isoprene, O<sub>3</sub>, NO<sub>x</sub> (= nitric oxide, NO, + nitrogen dioxide, NO<sub>2</sub>), MCR, and MVK (Griffin et al., 2002), no further detailed simulations solely of gas-phase chemistry were performed to test the original CACM module. Instead, a series of simulations was performed to investigate specifically the changes summarized above. In the following description, HV represents a scaling factor for availability of light, and concentrations represent those at the start of the simulation. Here, three cases were run to test the various regimes possibly affected by the chemical changes described above. Again, these cases were used simply to test the model hypothetically. In all cases, the initial isoprene mixing ratio is 0.1 ppm. The first case (Test1) represents a high-NO<sub>x</sub> daytime case in which HV = 0.5, [OH] = 6.1E-8 ppm, [O<sub>3</sub>] = 0.046 ppm, [NO] = 0.0334 ppm, and [NO<sub>2</sub>] = 0.0167 ppm. Test 2 is the same, except [NO] = [NO<sub>2</sub>] = 0; this case is designed to illustrate potential daytime RO<sub>2</sub>-HO<sub>2</sub> and RO<sub>2</sub>-RO<sub>2</sub> reaction regimes. Finally, Test 3 represents a nighttime test (HV = 0.0, [OH] = 0.0, [NO<sub>3</sub>] = 1.0E-5 ppm, and [O<sub>3</sub>] = 0.02 ppm) designed to provide information regarding the isoprene-NO<sub>3</sub> reaction sequence.

First, comparisons were made amongst all cases to ensure that only appropriate species were present: for example, to ensure that no nitrogen-containing species were formed in the case in which the total nitrogen oxide concentration was zero. To illustrate, Figure 2 shows concentrations of several species in the three test scenarios. Of most importance for this discussion are OOH6101 (far left in right panel) and OOH6102 (far right in right panel) (isomers of ISOPOOH) and IEPOX (second from right in left panel). As would be expected based on the lack of NO<sub>x</sub> during Test 2 and the lack of photochemistry in Test

3, Test 1 showed the smallest concentrations of OOH6101, OOH6102, and IEPOX. The lack of  $\text{NO}_x$  favors  $\text{RO}_2\text{-HO}_2$  reactions, which are required for the formation of the ISOPOOH isomers, which are precursors of IEPOX.

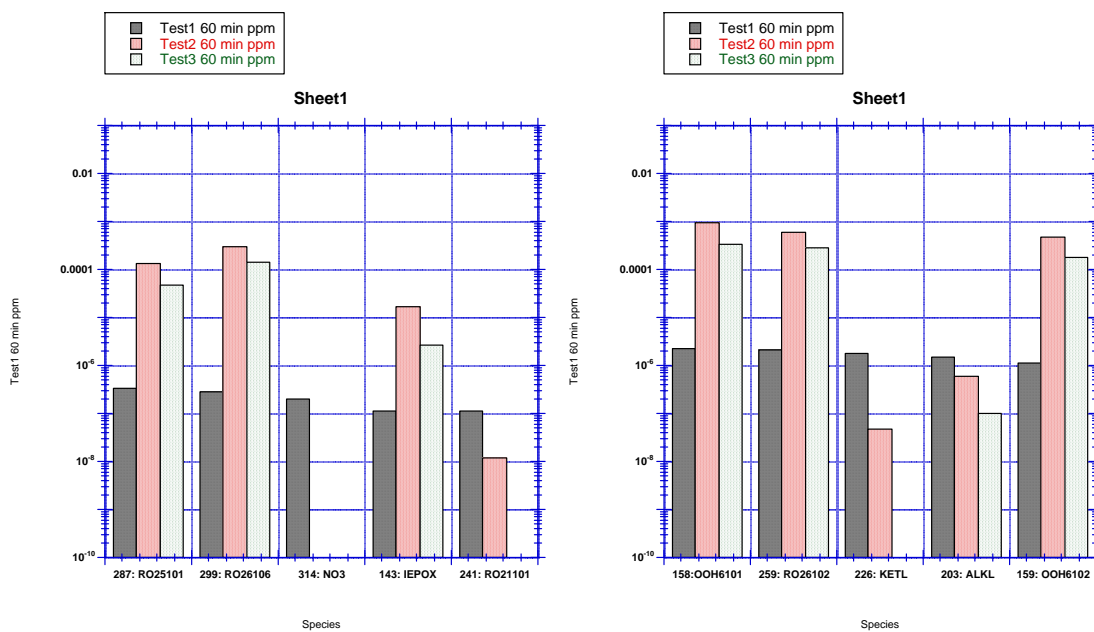


Figure 2. Comparison of important species between the three modeling scenarios used to validate changes made to CACM isoprene chemistry. Results are shown after one hour of simulated time. Gray: Test 1; Pink: Test 2; Light blue: Test 3. The y-axis is concentration (logarithmic scale) in ppm.

In theory, one could include data such as those included in Figure 2 for every modeled species. However, instead, a focus is placed here on specific compounds in order to highlight the potential influence of new compounds. Again, because this section is only serving to validate the new chemistry included in CACM, no aerosol results are yet included. As a first comparison between the cases, products of the  $\text{RO}_2\text{-NO}$  reaction that do not form SOA and the NV from MCR oxidation are compared (Figure 3). As would be expected, these products (besides that from MCR oxidation) are only formed in Test 1.

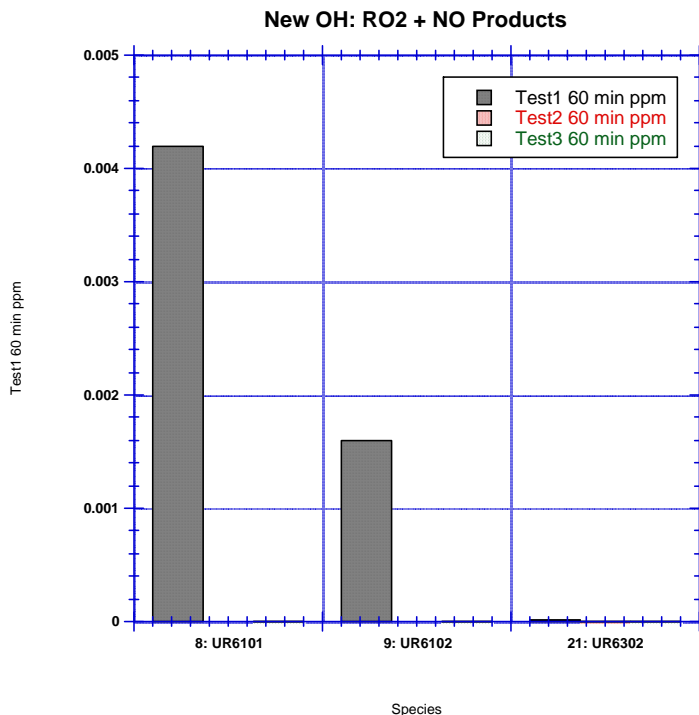


Figure 3. New products from the RO<sub>2</sub>-NO pathway. UR6101 represents hydroxynitrates and UR6102 represents hydroxycarbonyls from peroxy radicals formed from OH-oxidation of isoprene. UR6302 represents the NV product from MCR. UR6101 and UR6102 are not formed in Tests 2 or 3 (no NO). UR6302 is present in all cases and will be shown more clearly in subsequent figures. It differs by an order of magnitude between each test, with Test 1 > Test 2 > Test 3. Color scheme and simulation time identical to Figure 2.

Figure 4 similarly shows the new products in the RO<sub>2</sub>-HO<sub>2</sub> pathway. As expected, Test 2 (daytime, [NO] = 0.0) produces the largest concentrations observed in these tests for this set of products (peroxides and peroxide-derived products). Nonetheless, Test 3 (nighttime case) produces significant amounts (much larger than those for Test 1) of several of these products, particularly the hydroperoxides OOH6101 and OOH6102. Note, for comparison, the MCR aerosol product (UR6302) is relatively unimportant here, as it was for the RO<sub>2</sub>-NO system.

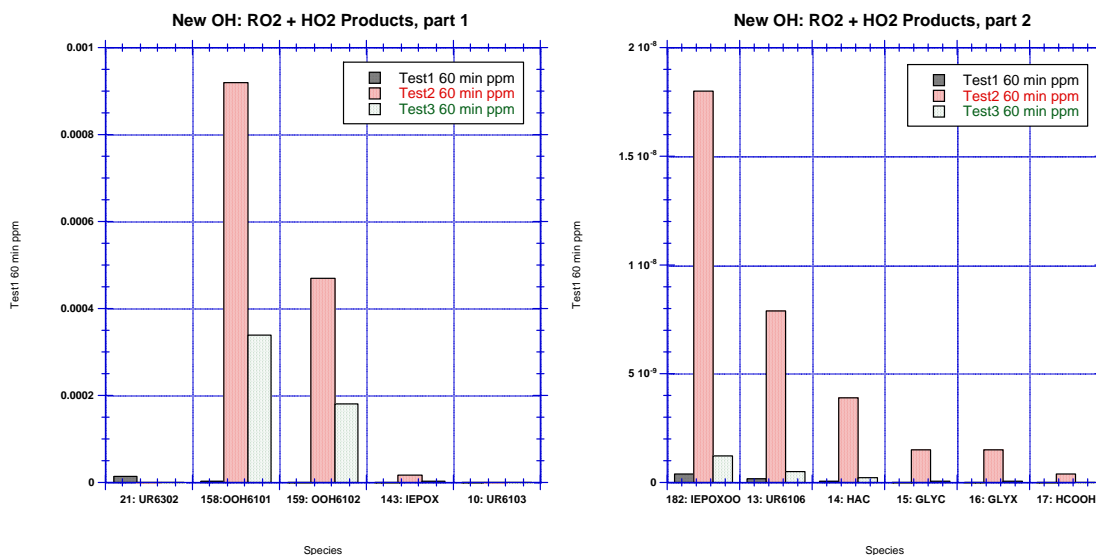


Figure 4. New products from RO<sub>2</sub>-HO<sub>2</sub>, shown split into two panels given the large number of new products here. Color scheme and simulation time identical to Figures 2 and 3.

Figure 5 shows the new product added to the RO<sub>2</sub>-RO<sub>2</sub> pathway; this product was included to test the significance of this pathway for SOA formation compared to the RO<sub>2</sub>-HO<sub>2</sub> pathway. Here, only one product that produces aerosol (UR6104) has been added. Very little of this product is formed in Test 1, but more of this is formed in Test 2 and Test 3 than the MCR aerosol product (UR6302). This may well indicate an enhancement of aerosol production under low-NO<sub>x</sub> conditions. However, the enhancement may well be insignificant given how little UR6302 forms in comparison to the RO<sub>2</sub>-HO<sub>2</sub> products (Figure 3). Again, adjustments to stoichiometric values for the NV products will be discussed in the MPMPO section. The changes made here are simply illustrative and are used to demonstrate the appropriateness of the gas-phase model behavior.

The last pathway to examine is that of nighttime isoprene plus NO<sub>3</sub> chemistry, specifically the RO<sub>2</sub>-RO<sub>2</sub> pathway (Figure 6). The only compound that forms in large

quantities is the new  $\delta$ -ISOP-NRO<sub>2</sub> (RO26108) in the initial reaction. In fact, the largest concentration of this forms in the high-NO<sub>x</sub> daytime case (Test 1), which makes sense because at the end of the simulation in the daytime case, [NO<sub>3</sub>] = 2.0E-7 ppm, while at night (Test 3), [NO<sub>3</sub>] = 9.7E-14 ppm because NO<sub>3</sub> is consumed but not regenerated. The only compound shown in Figure 6 that is produced in Test 2 is the MCR aerosol product, which must come from the pathways described previously. This makes sense because no NO<sub>x</sub> is present in Test 2 or Test 3.

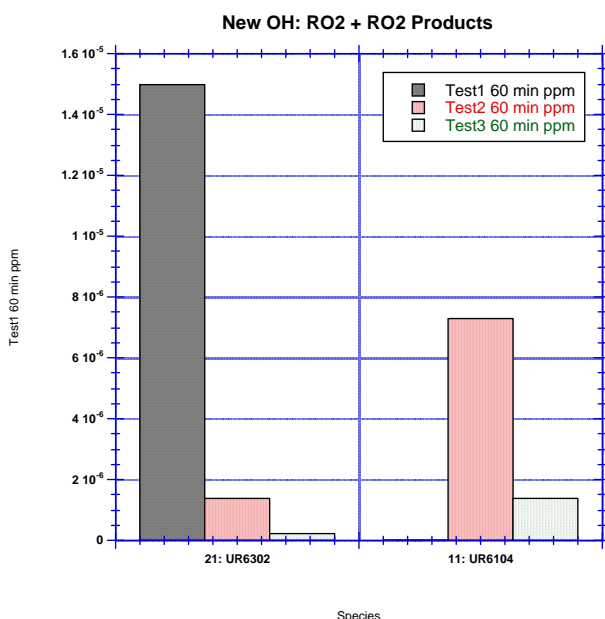


Figure 5. New products from the RO<sub>2</sub>-RO<sub>2</sub> pathway. Color scheme and simulation time identical to Figures 2 through 4.

However, Test 3 exhibits more of the hydroxynitrate (C<sub>5</sub>HN) and nitrooxycarbonyl (C<sub>5</sub>NC) produced from RO26108 because more other RO<sub>2</sub> is present in Test 3 at the end of the simulation compared to Test 1. Finally, none of the second-generation product anticipated to contribute to SOA forms during Test 3. This is due to not running the simulation for a longer period of time and having so little NO<sub>3</sub> left at the end of Test 3. A

very small amount of both RO26109 and UR6105 forms for Test 1; these result from the reaction of C5HN with NO<sub>3</sub>. This is due to the presence of significantly more NO<sub>3</sub> at the end of Test 1. In light of this, it would be expected that a simulation over multiple hours with more NO<sub>3</sub> would result in more nighttime formation of these products.

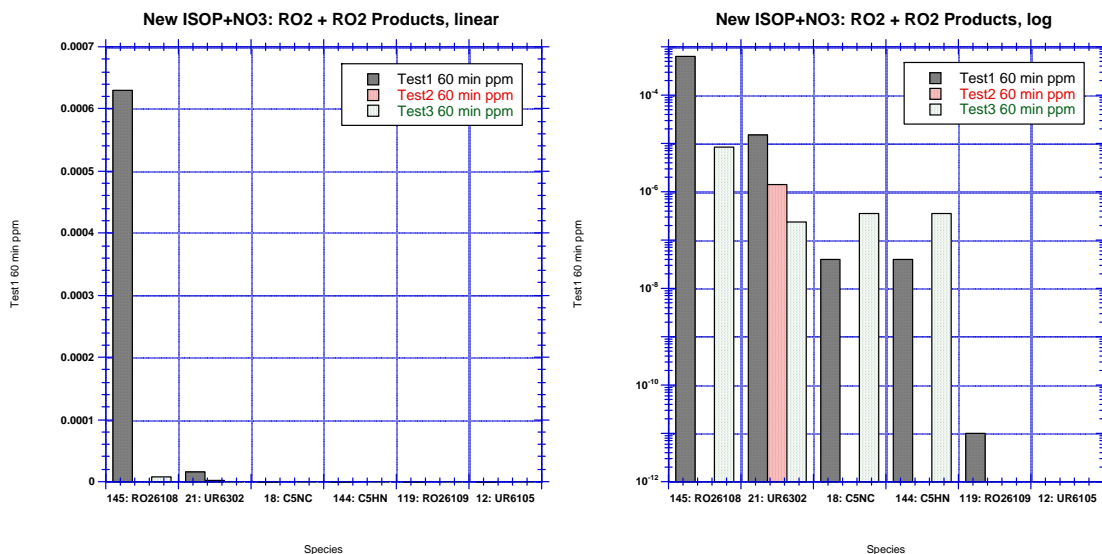


Figure 6. New products from isoprene-NO<sub>3</sub>: RO<sub>2</sub>-RO<sub>2</sub> pathway. Here both panels show the same products on different scales (linear on left, logarithmic on right). Color scheme and simulation time identical to Figures 2 through 5.

### *MPMPO*

Here, results are presented for scenarios based on low-NO<sub>x</sub> (Kroll et al., 2006), high-NO<sub>x</sub> (Kroll et al., 2006), and NO<sub>3</sub>-dominated chemistry (Ng et al., 2008). Actual chamber experiments are being simulated so both gas- and aerosol-phase data are presented.

### *Low-NO<sub>x</sub>*

Here the chamber experiment reported in Kroll et al. (2006) depicted in Figure 7 is simulated. Figure 7 shows that ~10 ppb of isoprene remains after two hours; this value is used to determine the initial concentration of hydrogen peroxide (H<sub>2</sub>O<sub>2</sub>), which was used

as an OH source. Based on this, the initial conditions for the simulation are [isoprene] = 0.0636 ppm, [NO<sub>x</sub>] ~ 0, [H<sub>2</sub>O<sub>2</sub>] = 0.8 ppm, and T = 300 K.

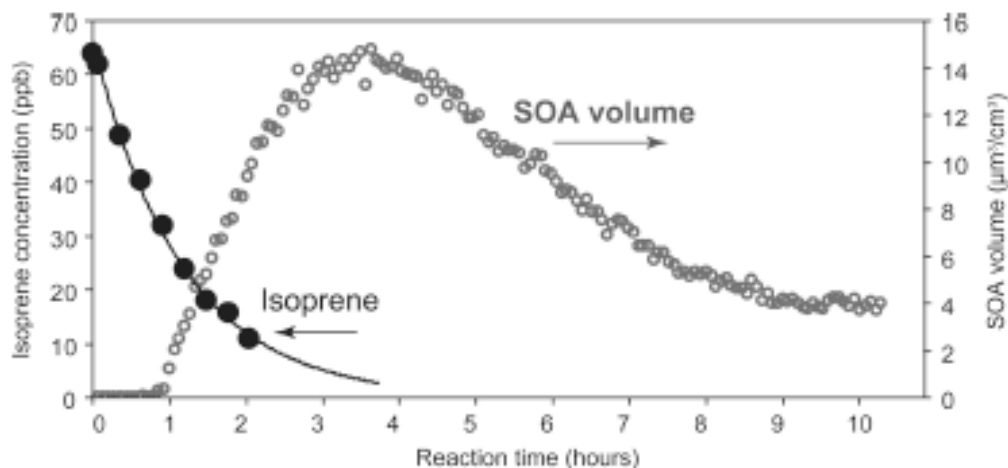


**FIGURE 2. Reaction profile of a typical isoprene photooxidation experiment under NO<sub>x</sub>-free conditions (Experiment 5).**

Figure 7. Experimental data for the low-NO<sub>x</sub> scenario taken from Kroll et al. (2006).

Figure 8 shows simulation results for the gas-phase only test (i.e., no partitioning allowed). Isoprene, MCR, MVK, and O<sub>3</sub> are shown. Kroll et al. (2006) note that a few ppb of O<sub>3</sub> were observed in the chamber. Slightly more is simulated here after 10 hours (approximately the length of the experiment). As expected, more MVK is produced than MCR. Figure 9 shows the simulated concentrations of H<sub>2</sub>O<sub>2</sub> and OH with HV = 1 in the simulation. There is a sufficient source of oxidant throughout the experiment.

Initially, the hydroperoxides (dark green curves, Figure 10) exhibit the largest concentrations, as they form from the RO<sub>2</sub>+HO<sub>2</sub> pathway. These compounds go on to react with OH, producing epoxides and other compounds that do not contribute to SOA. As a result, the hydroperoxides exhibit a steep decrease after isoprene (their source) is

sufficiently depleted. Similarly, the epoxide (teal curve, Figure 10) exhibits a rapid increase initially, ultimately exceeding the hydroperoxides in concentration by about 110 minutes and achieving their largest concentration at 200 minutes. This is followed by a slower decline (once their hydroperoxide source has largely reacted away) as they also react further with OH, producing either a NV product (UR6106, light green curve, Figure 10) or several products that remain in the gas-phase. The NV product from the epoxide (presumably an oligomer but here represented by a C<sub>10</sub> hemiacetal) steadily increases in concentration throughout the simulation, reaching a constant value of about 0.01 ppm at about 400 min after its epoxide source has been depleted completely.

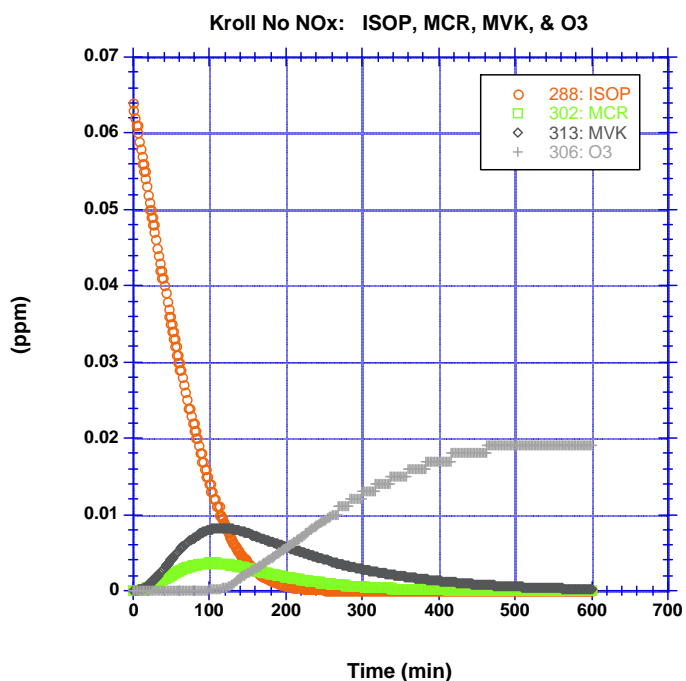


Figure 8. Isoprene, MCR, MVK, and O<sub>3</sub> concentrations during a gas-phase only 10-hour simulation based on experiment 5 reported in Kroll et al. (2006).

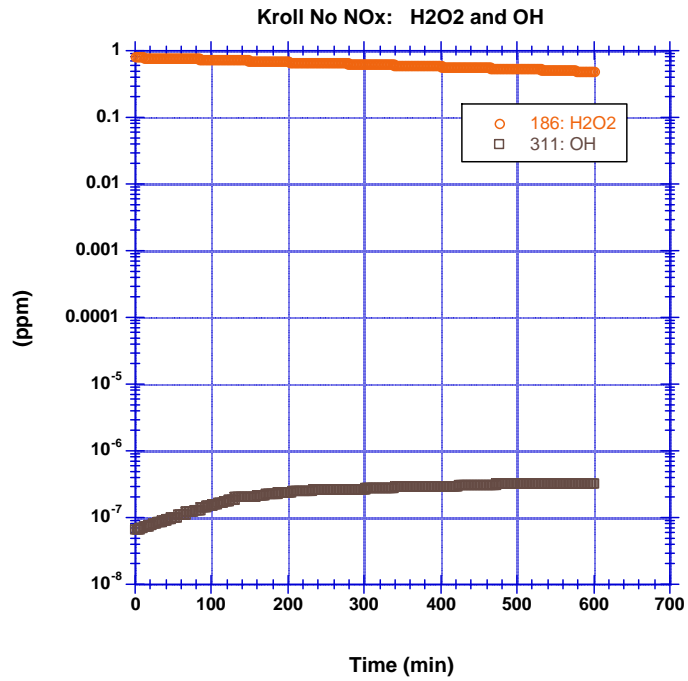


Figure 9. Simulated H<sub>2</sub>O<sub>2</sub> and OH as in Figure 8.

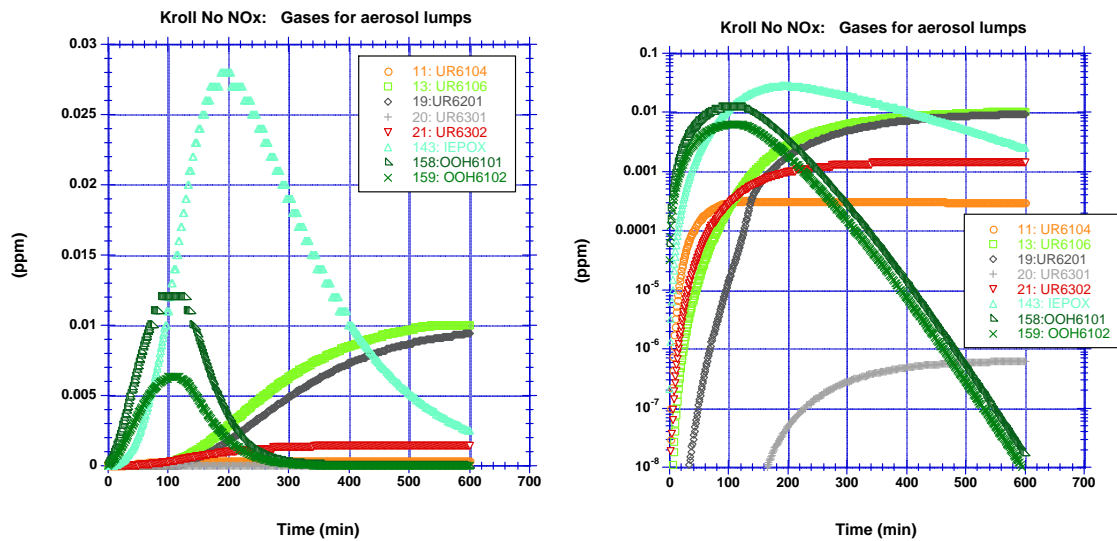


Figure 10. Simulated gases that contribute to the isoprene-related SOA lumps (linear scale on left, log scale on right) as in Figure 8. See text for details.

Two compounds shown in gray (UR6201 and UR6301) represent a previous lump (#6, not part of the newly added chemistry, discussed as UR21 in the context of Figure 1). These derive from O<sub>3</sub> reactions with MVK and MCR, respectively. The MVK product reaches the same concentration as the epoxide NV by the end of the simulation. The slight inflection in the shape of the curve at about 110 minutes reflects the time when O<sub>3</sub> is observed to begin increasing significantly (Figure 8). The MCR product is very minor, remaining less than 1E-6 ppm throughout the simulation (right panel, Figure 10).

UR6302 (red curve, Figure 10) represents NV that derives from MCR. This is particularly important under high-NO<sub>x</sub> conditions, but it also appears here due to the presence of MCR that arises from other pathways. Finally, UR6104 (orange curve, Figure 10) represents NV that arises from RO<sub>2</sub>+RO<sub>2</sub> reactions. These make only a minor contribution to the total gas-phase concentration here.

In the next simulation, these products are allowed to partition to the aerosol. This is particularly challenging because under these conditions, SOA was observed to increase rapidly then decrease due to photochemical processing (Kroll et al., 2006). This is not understood, so no attempt to account for this is included in the current work. Hence, the final SOA mass and yield given in Kroll et al. (2006) are used as target values:  $M_o$  equal to 5 µg/m<sup>3</sup> and SOA yield equal to 2.8%. Including aerosol formation had no appreciable effect on isoprene, MCR, MVK, O<sub>3</sub>, H<sub>2</sub>O<sub>2</sub>, or OH gas-phase concentrations.

Using the nominal vapor pressures, calculated as described previously using structure-activity relationships, there was insufficient mass to condense into aerosol. Based on a preliminary high-NO<sub>x</sub> test, the vapor pressure of UR6302 (the NV that derives from OH oxidation of MCR) was clearly too high to represent properly a NV species. Reducing its vapor pressure by a factor of 50 made enough of a difference for aerosol to form.

Here, little difference is seen between Figures 10 and 11 for the hydroperoxides, the epoxides, and the MVK+O<sub>3</sub> product UR6201. However, the gas-phase concentrations of UR6302 (red from MCR), UR6104 (orange from RO<sub>2</sub>+RO<sub>2</sub>), and UR6106 (green from epoxides) clearly are reduced, as they partition to the aerosol-phase.

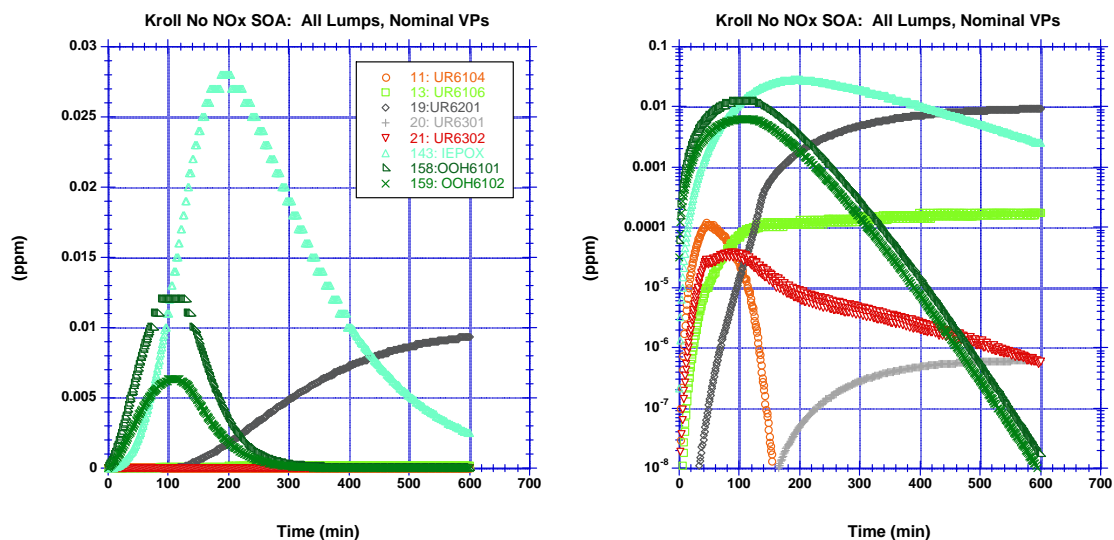


Figure 11. Simulated gases that contribute to the isoprene-related SOA lumps (linear scale on left, log scale on right) as in Figure 8. Here SOA is allowed to form using all isoprene-related lumps and the nominal vapor pressures (with the exception of UR6302, see text for details).

Nonetheless very little aerosol actually forms in this simulation (Figure 12, left panel).

Most of the mass remains in the gas-phase (CSOAT is the variable name in the model for

the sum of concentrations of gases that contribute to aerosol, expressed in units of  $\mu\text{g}/\text{m}^3$ , green curve Figure 12). In fact a log scale (Figure 12, right panel) is required to see what is happening with  $M_o$ , the total aerosol mass (orange circles, Figure 12, right panel). Here, both  $M_o$  and the sum of the individual contributions of each aerosol lump (Total Aerosol, gray diamonds) are plotted to verify that  $M_o$  is being calculated correctly. Clearly, there is a problem with  $M_o$ . Rather than a smooth curve, there are approximately 3 parallel curves. This was traced to a convergence problem in the calculation of  $M_o$ . Multiple possibilities for the source of the error were considered and tested. In the end, the problem was simply one of insufficient mass. Decreasing the vapor pressure of UR6302 by a factor of 50 as mentioned previously had provided enough mass for the  $M_o$  calculation to occur, but just barely. As a result, the convergence was highly sensitive to the initial values used in the iteration. Increasing the mass resolves the problem.

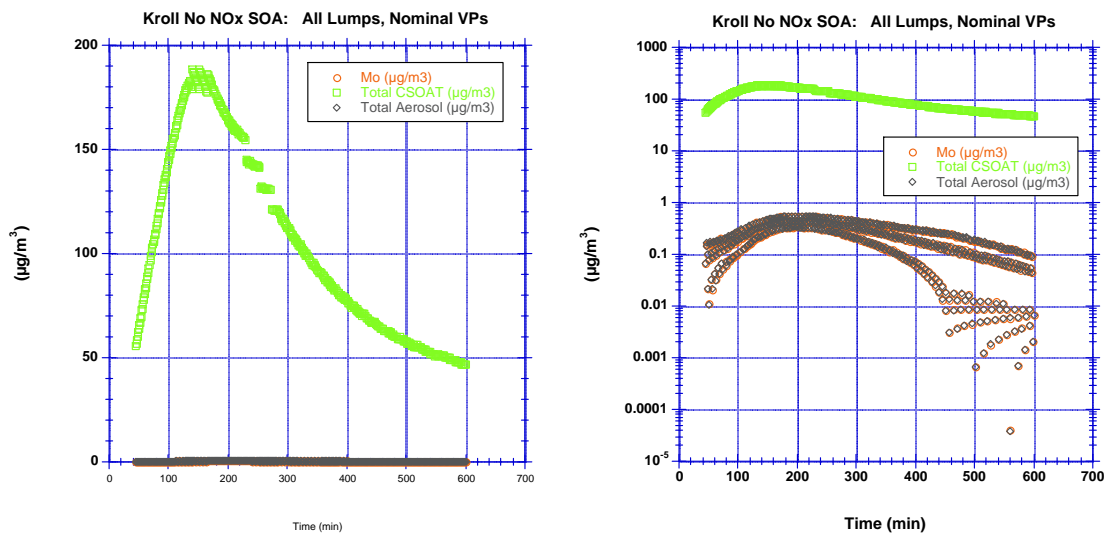


Figure 12. Total gas-phase concentration of all gases contributing to aerosol-phase (CSOAT, green squares) shown with total aerosol-phase concentration expressed both as  $M_o$  (orange circles) and total aerosol (gray diamonds) as in Figure 8.

Increasing the aerosol mass requires either decreasing the vapor pressures of the compounds contributing to the aerosols or increasing their gas-phase formation in CACM. First consider the vapor pressures. By definition, UR6302, UR6104, UR6106 (there is a 4<sup>th</sup>, UR6105, but it only appears in the presence of NO<sub>x</sub>) are intended to represent NV products (i.e., they should exist entirely in the aerosol phase) from various gas-phase mechanisms. Although there is a convergence problem in this simulation, a quick check of the fraction of the total concentration of each SOA lump partitioning to aerosol gives a sense of whether the vapor pressures used for these compounds are sufficient to drive them into the aerosol-phase. The data shown in Figure 13 indicate that the three NV products here reside primarily in the gas phase (aerosol fractions less than 0.35). Figure 13 also suggests that only a minuscule amount of hydroperoxide (dark green diamonds) partitions to aerosol, with epoxides and MVK+O<sub>3</sub> product (UR6201) contributing only marginally more to aerosol.

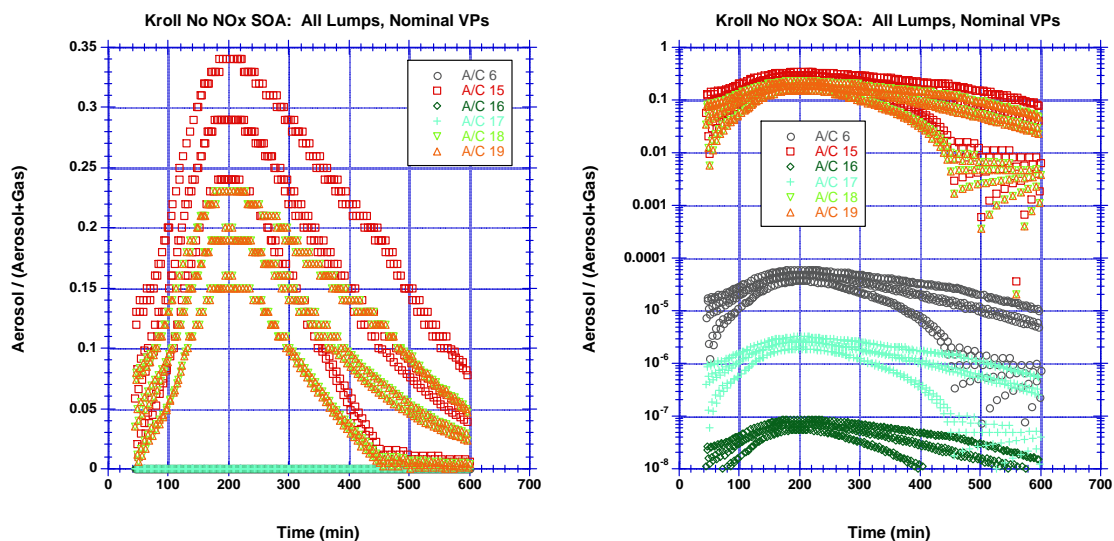


Figure 13. Preliminary checks of the partitioning between the aerosol- and gas-phases for each isoprene-related SOA lump using the aerosol fraction.

To test whether or not there is sufficient mass if vapor pressures are low enough, the vapor pressures of UR6302, UR6106, and UR6104 were all decreased by  $1E4$ . First, more mass clearly resolved the convergence problem in aerosol mass (Figure 14) as one curve properly has replaced the parallel set of curves. Second,  $M_o$  and total aerosol are again the same as they should be. Third, by the end of the simulation,  $5.5 \mu\text{g}/\text{m}^3$  of aerosol has formed, which is essentially the target value. Interesting features can be seen in the  $M_o$  curve in Figures 14 and 15.

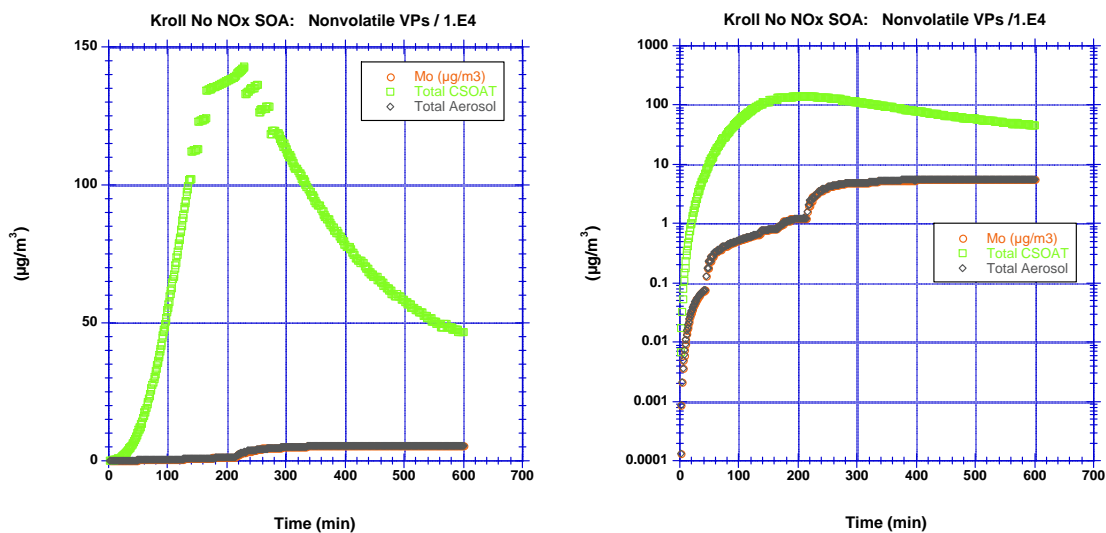


Figure 14. Total gas-phase concentration (CSOAT in green) shown with total aerosol concentration ( $M_o$  and total aerosol, orange and gray, respectively) as in Figure 8 but with decreased vapor pressures.

The total aerosol concentration starts to increase appreciably at approximately 40 minutes into the simulation (Figures 14 and 15, left panel), consistent with the observations that aerosols appeared in the chamber at this time (Kroll et al., 2006). Initially, the aerosol is dominated by the  $\text{RO}_2+\text{RO}_2$  NV (UR6104, orange curve, Figure 15). Isoprene is the source of these  $\text{RO}_2$  radicals; UR6104 no longer increases after isoprene is depleted sufficiently. Next both UR6302 (from  $\text{MCR}+\text{OH}$ ) and UR6106 (from epoxides) together

lead to an increase in total  $M_o$ . Presumably these follow the initial dominance of UR6104 because they derive from 1<sup>st</sup> (MCR) and 2<sup>nd</sup> (epoxides) generation products from isoprene. After 200 minutes, there is a dramatic increase in  $M_o$  nearly entirely due to increasing NV formation from epoxides (Figure 15).  $M_o$  levels off after about 400 minutes. It is encouraging that the model captures some of the key features observed in the laboratory and follows expectations from the gas-phase chemistry.

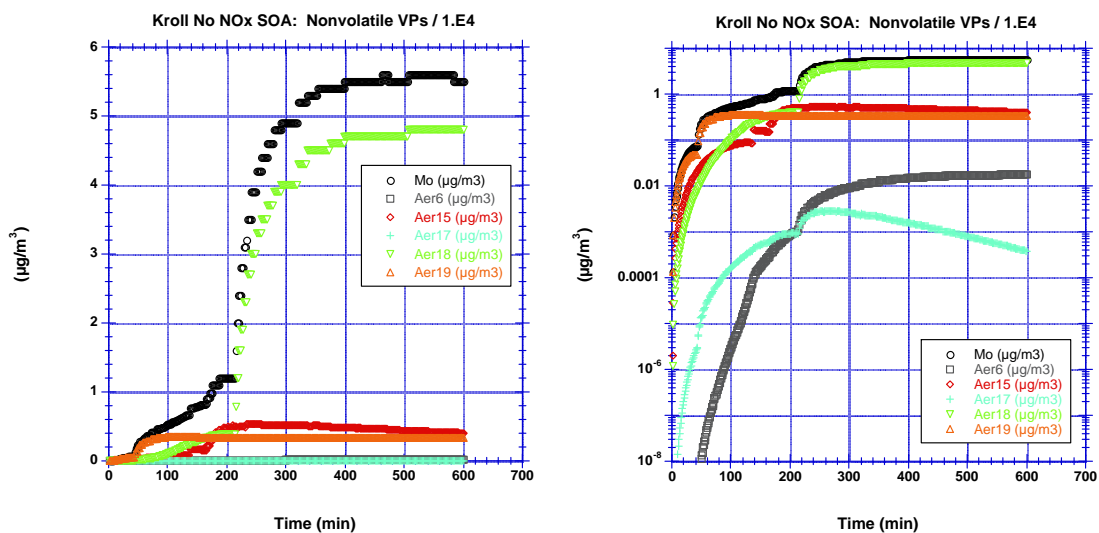


Figure 15. Total aerosol concentration ( $M_o$ ) and the contribution of each individual SOA lump (linear scale on left, log scale on right) as in Figure 14.

Note that in Figure 15, there is no reference to lump 16 (that used to simulate aerosol formed from hydroperoxide partitioning). From the log scale panel of Figure 15, it is clear that the epoxide contribution to the aerosol mass is approximately three to four orders of magnitude smaller than the total mass observed, a very tiny contribution. From earlier tests, the contribution to the total aerosol mass from hydroperoxides was another few orders of magnitude smaller than that of the epoxides. Therefore, hydroxyhydroperoxides are no longer included in the partitioning module of the code. In

Figure 16, the information originally given in Figure 13 is updated for the current simulation.

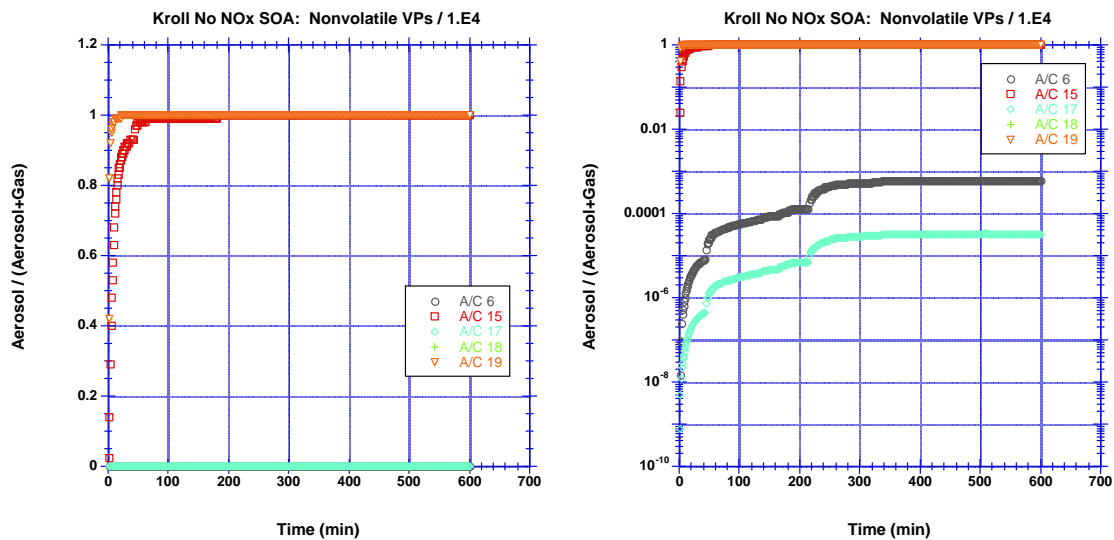


Figure 16. Fraction of the total concentration of SOA-forming compounds found in aerosol (linear scale left panel, log scale right panel as in Figure 15).

The gas-phase concentrations (ppm) show only compounds that exist primarily in the gas-phase (Figure 17). Meanwhile, other compounds such as isoprene, MCR, MVK, etc. continue to appear as they did in Figure 8.

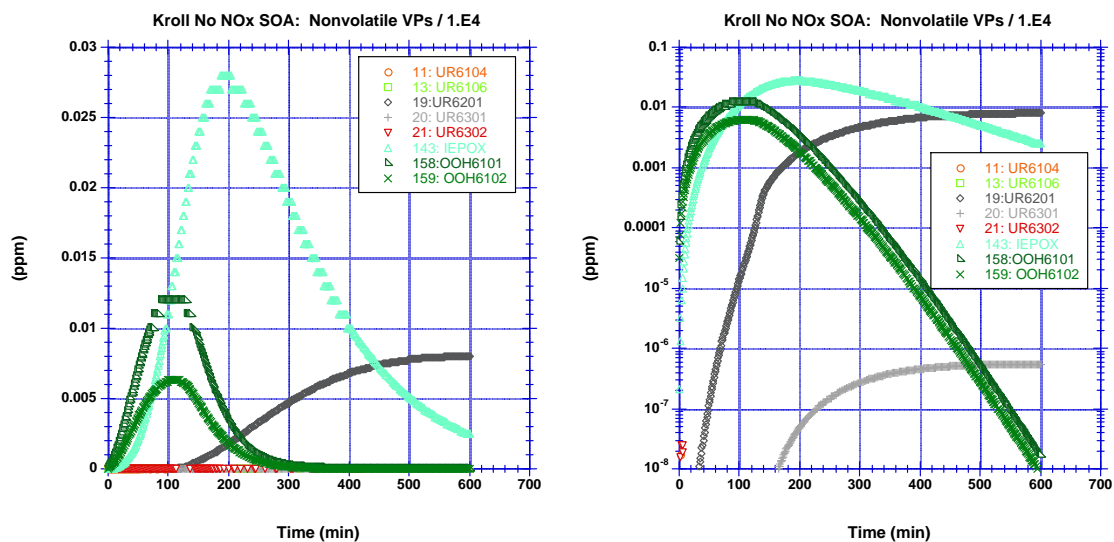


Figure 17. Gas concentrations (ppm) for compounds that contribute to SOA lumps.

Decreasing the vapor pressures of the NV products was a successful means of simulating the overall mass of SOA formed in the chamber (Figure 15). However, it should be determined if such a large decrease was necessary. An identical simulation to this one using a factor of 100 (instead of 1E4) only produced a maximum of  $0.45 \mu\text{g}/\text{m}^3$ . Similarly, a test of a factor of 1000 produced only  $3.5 \mu\text{g}/\text{m}^3$ , 30% below the target value of  $5 \mu\text{g}/\text{m}^3$ . Note that Kroll et al. (2006) give the final aerosol mass for this experiment as  $5.0 \pm 0.5 \mu\text{g}/\text{m}^3$ ; the current value is within the experimental error.

However, it must be noted that the amount of each of the NV species reported here is somewhat arbitrary. There is not good information about how much of any of the parent compounds ( $\text{RO}_2$  for UR6104, epoxides for UR6106, or MCR for UR6302) find their way into aerosol. It is assumed that 3% of the  $\text{RO}_2 + \text{RO}_2$  products form UR6104 based on comparable reactions of  $\text{RO}_2 + \text{RO}_2$  following isoprene oxidation by  $\text{NO}_3$  in the dark (Ng et al., 2008). For both UR6106 and UR6302 a value of 25% works well. Nonetheless, one ought to test the sensitivity to this choice. Based on the chamber studies reported by Kroll et al. (2006), Surratt et al. (2006), and Paulot et al. (2009), it is not expected that the MCR NV should comprise a large fraction of aerosol here, nor should the  $\text{RO}_2 + \text{RO}_2$  NV UR6104. Therefore, the only compound used to test the sensitivity of  $M_o$  and aerosol fraction ( $A/C$ , where A is the aerosol concentration and C is the total concentration) was UR6106, the NV that arises from epoxides.

In the studies just described a fraction of 25% and vapor pressures multiplied by 1E-4 were used. A smaller stoichiometric fraction will produce too little aerosol even at the very low vapor pressures used here. Considering larger fractions of 50% and 90% and higher vapor pressures (i.e., to see if more NV formation along with higher vapor pressures can do as well or better at matching the laboratory results), no matter how much NV is allowed to form from epoxides, a vapor pressure decreased by only a factor of 100 fails to reproduce both sufficient aerosol mass concentrations and the degree of partitioning to the aerosol to be considered a success. Therefore, a fraction of 25% and a vapor pressure reduced by four orders of magnitude are retained.

It should be noted that the vapor pressure changes simply may reflect that the dimers used here to represent the NV are too small molecularly. Perhaps trimers or larger compounds would be better. Whatever compounds may be the most representative, it is clear that these vapor pressures indicate the critical role that oligomerization and other possible particle-phase reactions play in forcing products of isoprene oxidation to form aerosol.

#### *High-NO<sub>x</sub>*

Here, the chamber experiment reported in Kroll et al. (2006) for high-NO<sub>x</sub> conditions (#11) depicted in Figure 18 is simulated. The initial conditions for this case are [isoprene] equal to 0.0427 ppm, [NO] equal to 0.098 ppm, [NO<sub>2</sub>] equal to 0.031 ppm, and a temperature of 301K. Ammonium sulfate seed particles were also included, but because such salts are neutralized fully, they do not affect the experiment or the

simulation. As with the low-NO<sub>x</sub> case, H<sub>2</sub>O<sub>2</sub> is the source for OH in the chamber. The data from Kroll et al. (2006) do not include isoprene. Therefore, it is assumed that the only difference between the high-NO<sub>x</sub> and low-NO<sub>x</sub> test cases is the presence of NO<sub>x</sub>, and the same initial value for H<sub>2</sub>O<sub>2</sub> (0.8 ppm) was used here. The results of this simulation are shown in Figure 19.

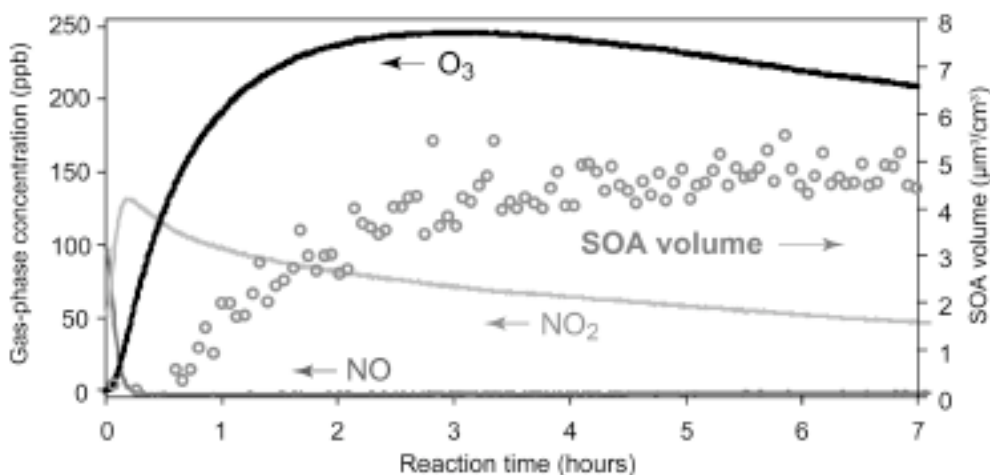


**FIGURE 5. Reaction profile of a typical isoprene photooxidation experiment under high-NO<sub>x</sub> conditions (Experiment 11). Decay of isoprene is rapid, with most consumed in the first 30 min of reaction, so it is omitted for clarity.**

Figure 18. Experimental data for the high-NO<sub>x</sub> scenario (Kroll et al., 2006).

Here isoprene is essentially gone after an hour (left panel, Figure 19). However, a comparison of the NO, NO<sub>2</sub>, and O<sub>3</sub> curves (right panel, Figure 19) with the Kroll et al. (2006) figure (Figure 18) indicates this simulation has insufficient oxidant. From Kroll et al. (2006), at ~ 20 minutes, NO is gone and NO<sub>2</sub> peaks at ~0.013 ppm. Further, O<sub>3</sub> reaches a maximum of nearly 0.025 ppm after about 2 hours, then slowly tapers off to approximately 0.020 ppm at the end of the study at 7 hours. In the simulation, NO is not removed until after an hour, NO peaks at approximately 0.08 ppm after 40 minutes, and

O<sub>3</sub> increases unabated throughout the simulation. The O<sub>3</sub> result suggests that either an additional initial concentration of some compound in the chamber has been overlooked or that the isoprene-related O<sub>3</sub> chemistry is incomplete. It could also be related to not capturing photolysis accurately given the uncertainty associated with the spectrum of the lights associated with the chamber. The fact that the simulation does not reflect the laboratory NO<sub>2</sub> peak in either magnitude or timing suggests that, with insufficient oxidant to quickly convert NO fully to NO<sub>2</sub>, other reactions take up NO<sub>x</sub> such that NO<sub>2</sub> never solely reflects the total initial value of NO<sub>x</sub> (0.131 ppm), as it does in the chamber.

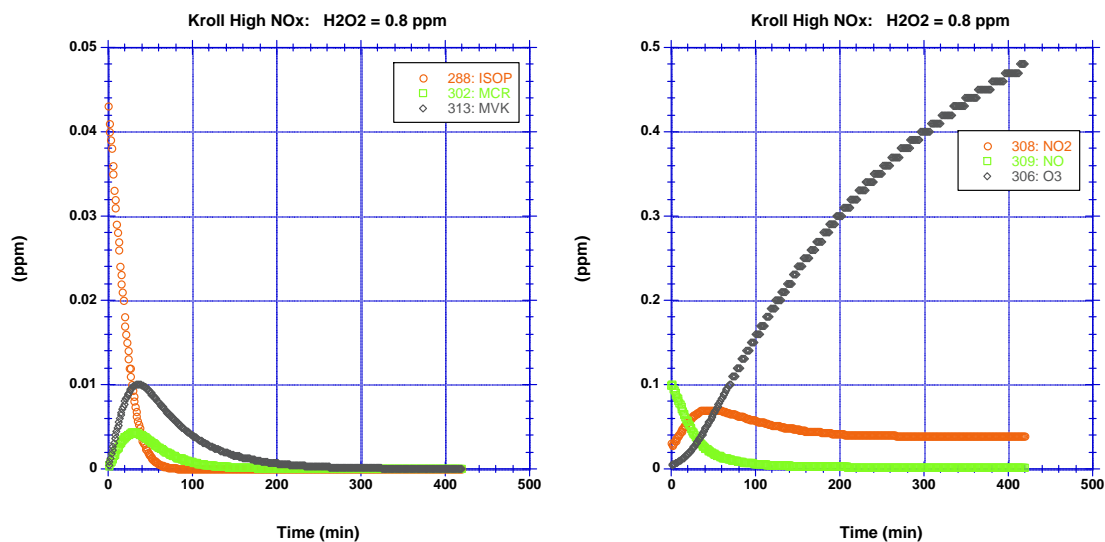


Figure 19. High NO<sub>x</sub> test case using same initial H<sub>2</sub>O<sub>2</sub> concentration as in the low-NO<sub>x</sub> test case.

A set of tests was conducted to look at the sensitivity of isoprene and NO<sub>x</sub> (setting aside the problem of reproducing O<sub>3</sub> for now) to initial H<sub>2</sub>O<sub>2</sub> concentrations in the simulations (Figure 20). Three initial concentrations were tested, H<sub>2</sub>O<sub>2</sub> = 0.1, 1.0, and 10.0 ppm. The smallest concentration of 0.1 ppm exacerbates the problems just described with removal of isoprene and conversion of NO to NO<sub>2</sub> occurring much too slowly. It is included only

for comparison to the other two cases of 1.0 and 10.0 ppm. The 1.0 ppm case is comparable to the 0.8 case just described. Here, isoprene is essentially gone by 40 minutes; a sharper peak in  $\text{NO}_2$  is observed, but it still remains too small compared to Kroll et al. (2006). In fact, in an effort to try to obtain a peak greater than 0.10 ppm,  $\text{H}_2\text{O}_2$  was increased to 10.0 ppm. Here,  $\text{NO}_2$  is seen to increase from its initial value of 0.031 ppm to  $\sim 0.095$  ppm (Figure 20) in one time step. It appears that the chemistry competing with this  $\text{NO}_x$  chemistry is fast and efficient throughout the simulation. As a result, no matter what initial concentration of  $\text{H}_2\text{O}_2$  is chosen, the magnitude of the  $\text{NO}_2$  curve will not be replicated. However, if an initial concentration of 1.6 ppm is used for  $\text{H}_2\text{O}_2$ , the timing of both the  $\text{NO}_2$  peak (at  $\sim 20$  minutes) and the removal of isoprene after 30 minutes can be captured (Figure 21). However, this choice results in a simulated  $\text{O}_3$  concentration that exceeds 0.4 ppm at 2 hours (compared to  $\sim 0.24$  ppm in the chamber) and continues to climb to 0.8 ppm by the end of the simulation at 7 hours (Figure 22, left panel). This may pose problems in simulating SOA formation in the chamber because  $\text{O}_3$  concentrations that exceed those observed in the chamber by over a factor of three might be expected to enhance SOA that derives from  $\text{O}_3$ -related reactions compared to the conditions that existed in the chamber. To test the sensitivity to  $\text{O}_3$  and to provide a comparison to the low- $\text{NO}_x$  simulation, two test cases will be employed for high- $\text{NO}_x$  SOA formation:  $[\text{H}_2\text{O}_2] = 1.6$  ppm to capture the timing of the isoprene consumption and  $[\text{H}_2\text{O}_2] = 0.8$  ppm to reduce  $\text{O}_3$  concentrations by half (Figure 22, right panel) from the former case and to provide a comparative study of the influence of  $\text{NO}_x$ .

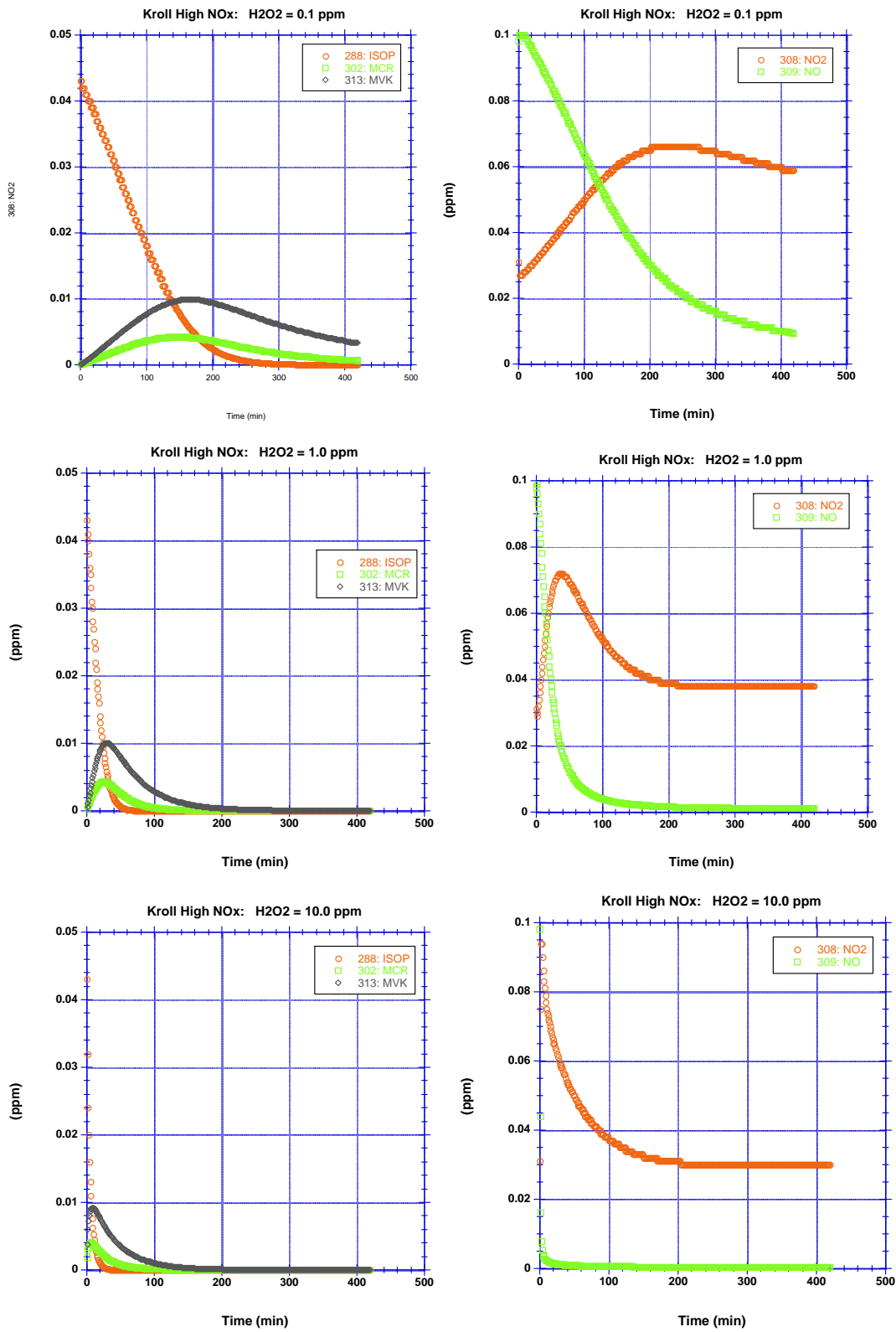


Figure 20. Tests of isoprene and NO<sub>x</sub> sensitivity to H<sub>2</sub>O<sub>2</sub> (and hence OH) concentrations as in Figure 19.

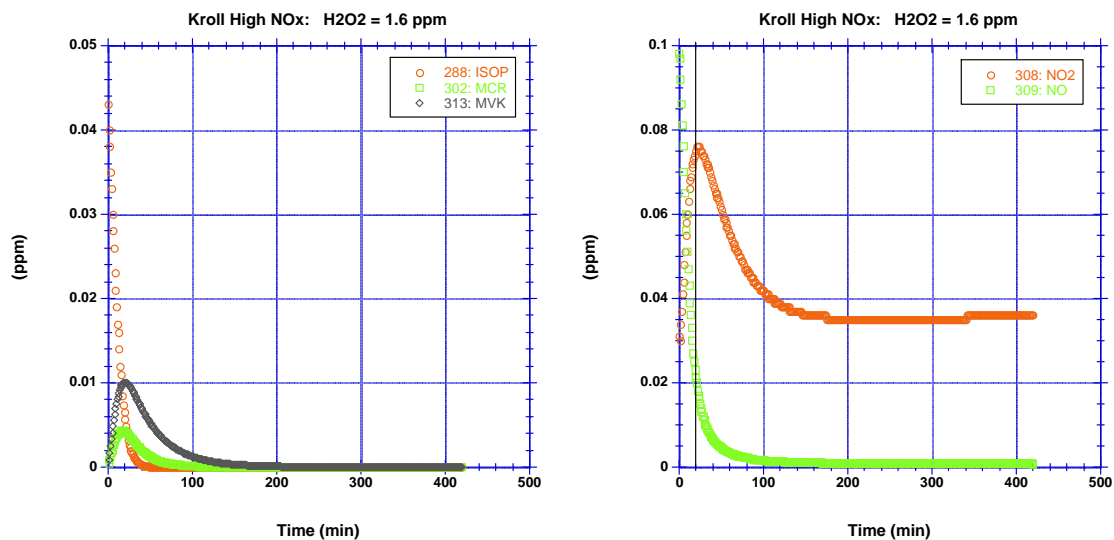


Figure 21. Simulation using  $\text{H}_2\text{O}_2 = 1.6$  ppm which reproduces the timing of the  $\text{NO}_2$  peak and the removal of isoprene as described by Kroll et al. (2006) as in Figure 19.

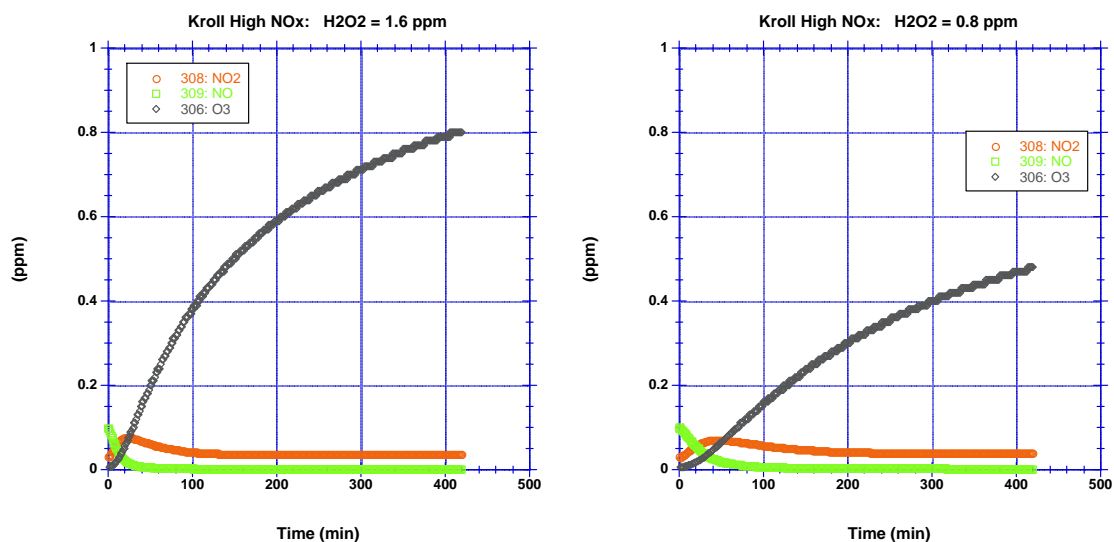


Figure 22. Comparison of simulated  $\text{O}_3$  depending on the initial concentration of  $\text{H}_2\text{O}_2$ : 1.6 ppm left panel, 0.8 ppm right panel as in Figure 19.

Overall, there is little difference between the gas-phase concentrations related to isoprene SOA formation between the two test cases (Figure 23). The NV that derives from MCR+OH (UR6302) dominates the gas-phase compounds here (red triangles, Figure 23). There is a slight enhancement in UR6201 and UR6301 (gray pluses and inverted

triangles, Figure 23), the compounds that derive from O<sub>3</sub> oxidation of MVK and MCR, respectively, in the case with more oxidant, as expected from the O<sub>3</sub> curves (Figure 22). However, these compounds are present at concentrations either 1% (UR6201) or many orders of magnitude smaller than that of UR6302. Hence, it is unlikely that there will be much difference in SOA formation between these two cases. Indeed, it is likely good agreement with the chamber aerosol data may be obtained.

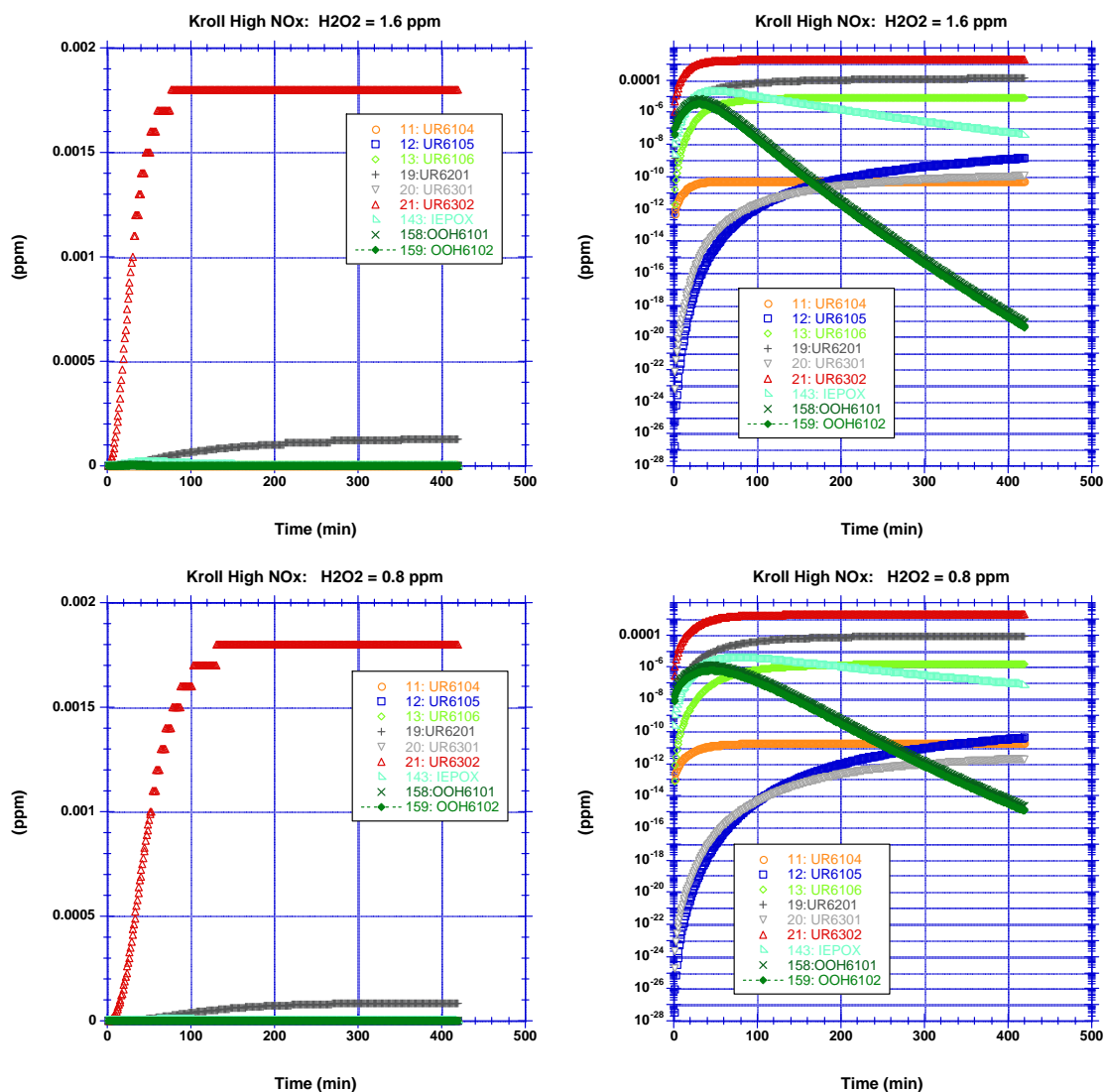


Figure 23. Simulated gases for isoprene-related SOA formation, left panels linear scale and right panels logarithmic scale, for the two test cases  $[H_2O_2] = 1.6$  ppm (top panels) and 0.8 ppm (bottom panels) as in Figure 19.

In general, as expected in the case with more oxidant, gas concentrations are observed to either be produced or depleted more quickly as the case may be (right panels, Figure 23). Also as expected, the hydroxyhydroperoxides, epoxides, and the epoxide NV are minor contributors under high-NO<sub>x</sub> conditions (Figure 23, lower right panel) compared to the low-NO<sub>x</sub> case (Figure 10). Finally note that there is an additional compound (UR6105) under high-NO<sub>x</sub> conditions that did not appear in the low-NO<sub>x</sub> case. This is an NV that arises from RO<sub>2</sub>+RO<sub>2</sub> reactions that proceed after isoprene is oxidized by NO<sub>3</sub>. In daylight, there is little NO<sub>3</sub> available to react with isoprene; hence, only a tiny amount of it appears here (blue squares, Figure 23).

Here, SOA was observed in the laboratory to accumulate over time reaching a constant concentration of  $6.7 \pm 1.3 \mu\text{g}/\text{m}^3$  after 4 hours and to persist until the end of the experiment at 7 hours. Hence, in this study the behavior of the simulation as a function of time as well as final outcome can be examined. Using the final result from the low-NO<sub>x</sub> case, i.e., the vapor pressures of UR6302, UR6106, and UR6104 decreased by 1E4 and that these NV species comprise 25%, 25%, and 3% of the products from their parent compounds, respectively, the SOA production from the high-NO<sub>x</sub> gas-phase chemistry as described above is simulated.

As one would expect, there are differences between the two H<sub>2</sub>O<sub>2</sub> cases, but they are minor. In the higher oxidant simulation the total aerosol ( $M_o$ ) is slightly larger and reaches its peak sooner than in the lower oxidant case (Figure 24). Unlike the low-NO<sub>x</sub> case (Figure 14), nearly all of the available mass (CSOAT, green squares, Figure 24)

partitions to aerosol (gray diamonds, Figure 24). Also unlike the low-NO<sub>x</sub> case, there is POA in the laboratory study, so its presence is simulated here. As a check on model performance,  $M_o$ -POA should equal SOA (labeled here as Total Aerosol, as in the low-NO<sub>x</sub> case). As shown in Figure 24, these two curves agree.

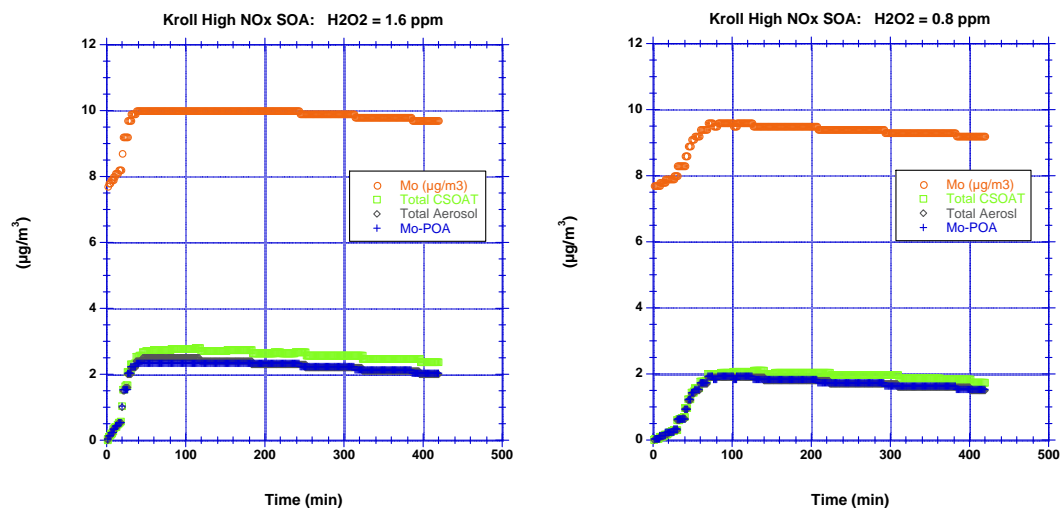


Figure 24. Comparison of total aerosol ( $M_o$ ), total concentrations (gas + aerosol, CSOAT), SOA, and the difference between  $M_o$  and POA.  $[H_2O_2] = 1.6$  ppm case on left,  $= 0.8$  ppm case on right.

Finally, a comparison of the contributions of the individual lumps to the total SOA makes clear that the excess O<sub>3</sub> in the simulations is not influencing unduly aerosol formation (Figure 25). In both cases, SOA is entirely due to the NV formed from MCR+OH (UR6302). The NV from epoxides (UR6106) contributes <1% to the total; all other contributions are one to six orders of magnitude smaller. Therefore, the  $[H_2O_2] = 1.6$  ppm case can be considered safely to be representative of the chamber data on the basis of the timing of the NO<sub>2</sub> peak and the removal of isoprene. If O<sub>3</sub> were a major factor in the SOA here, it would be reflected in lump 6, which derives from O<sub>3</sub> oxidation of MVK and MCR. This is seen clearly in the gas-phase concentrations, in which the

concentration of UR6201 is second only to UR6302 (Figure 23), though it is a distant second, an order of magnitude smaller than that of UR6302. For SOA, lump 6 is even less important, four orders of magnitude smaller, due to its relatively limited partitioning to aerosol (Figure 26). Even with this limited role, it is the third most prevalent compound in the high-NO<sub>x</sub> case, following the contribution of epoxide NV (UR6106).

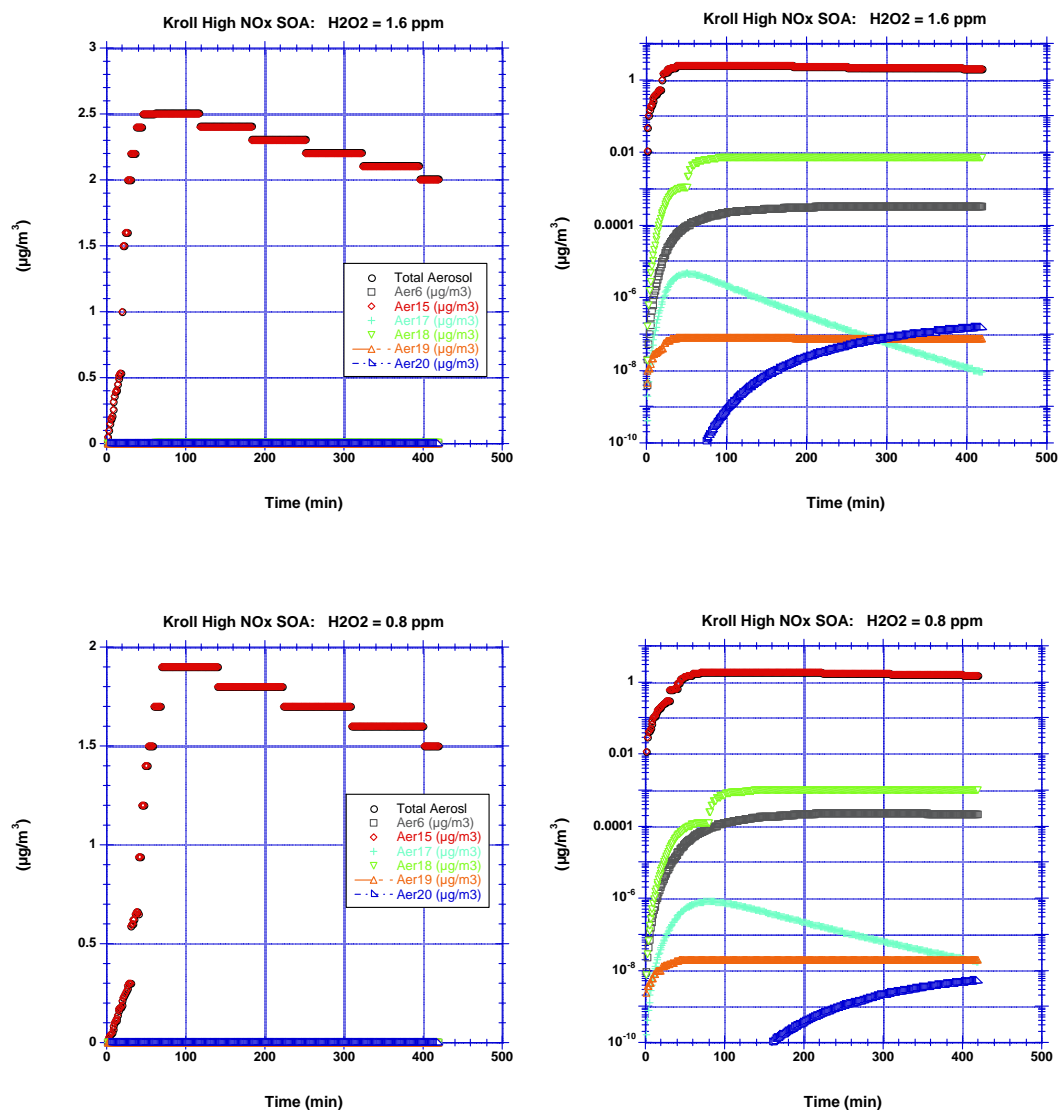


Figure 25. Comparison of contributions of each SOA lump to the total aerosol present, left panels linear scale, right panels logarithmic scale, for the H<sub>2</sub>O<sub>2</sub> cases: 1.6 ppm (top panels) and 0.8 ppm (bottom panels) as in Figure 24.

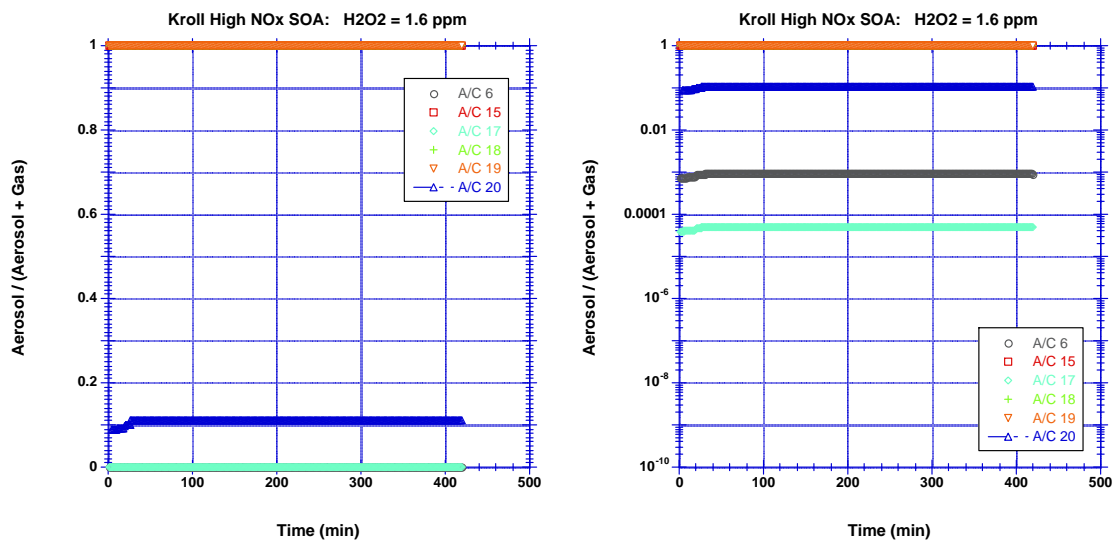


Figure 26. Fraction of total mass concentration found in aerosol, linear scale on left, log scale on right as in Figure 24. UR6302, UR6106, and UR6104 all partition completely (100%) to aerosol; hence, they over plot each other with only lump 19 (UR6104) visible.

On this basis, the  $[H_2O_2] = 1.6$  ppm case will be treated as the proper basis for comparison to the chamber because it was designed to match the gas-phase changes in isoprene and  $NO_2$ . However, here there is disagreement with the chamber data in Figure 18. In the laboratory, aerosol does not appear until the isoprene is nearly consumed. It increases steadily for 2 hours until it reaches a fairly constant concentration for the remainder of the experiment. In these simulations, aerosol mass accumulates from the beginning, rising quickly to its maximum value at the end of an hour, then slowly decreases until the end of the simulation (Figure 25). This suggests that the parameterization in which  $MCR + OH$  produces the NV product, along with its other known gas-phase products is not optimal. It likely would be better to delay its occurrence for another generation or two to capture more accurately the onset and slower accumulation of SOA from this product. Unfortunately, there is insufficient chemical understanding of the processes that give rise to this product (Surratt et al., 2006). Hence,

for now, this chemical implementation will remain unchanged until a future date when more detailed chemical descriptions of SOA deriving from MCR are available.

In addition to the timing of onset and the shape of the SOA curve in this simulation, there is clearly insufficient mass being formed. The target value observed in the laboratory was  $6.7 \pm 1.3 \mu\text{g}/\text{m}^3$ . Here the final SOA from the  $[\text{H}_2\text{O}_2] = 1.6 \text{ ppm}$  case is  $2.02 \mu\text{g}/\text{m}^3$ . Here, UR6302 is partitioning completely (100% throughout the simulation, Figure 26), as are the other NV species except for UR6105, which did not appear in the low- $\text{NO}_x$  case, so its vapor pressure was not adjusted. Here only a fraction ( $\sim 10\%$ ) contributes to the aerosol. For the sake of consistency, its vapor pressure should also be decreased by  $1\text{E}4$  to force it all into aerosol as with the other NV species.

Because adjusting the vapor pressure is already causing all of the UR6302 mass to go into aerosol, the only available avenue to increase the mass to the target value is to increase the rate of formation. Here it represents 25% of all products from MCR+OH. As noted in the low- $\text{NO}_x$  case, this was determined by fitting. An increase from 25% to 70% is sufficient to simulate the target value of  $6.7 \pm 1.3 \mu\text{g}/\text{m}^3$ , with a final simulated SOA concentration of  $6.31 \mu\text{g}/\text{m}^3$  (Figure 27). At this time, it is unclear why such a dramatic change in this factor is necessary between the two scenarios. It may be related to reactions between MCR and  $\text{NO}_3$  also leading to the equivalent NV and hence SOA. This possibility is being explored currently as this report is being converted to a scientific manuscript.

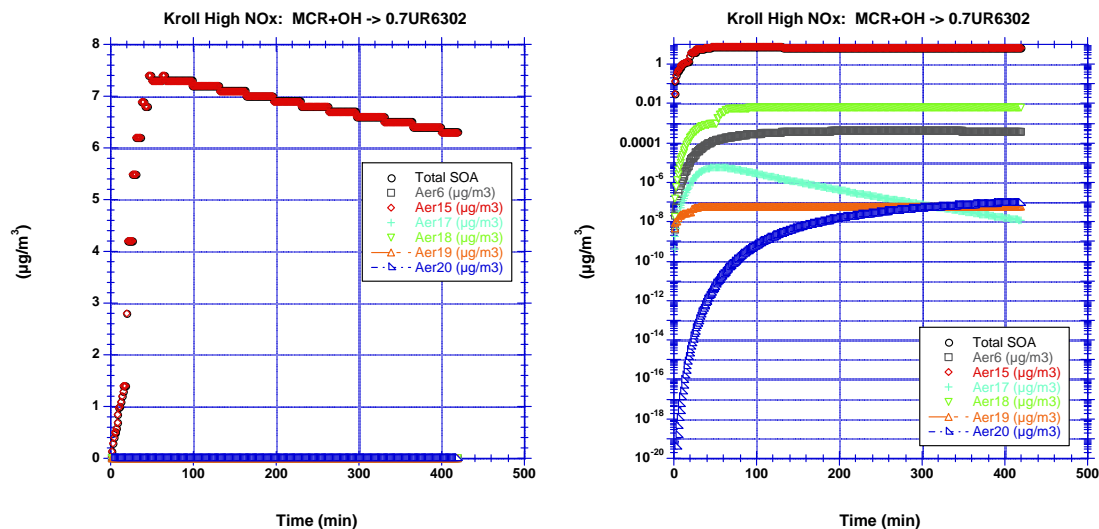
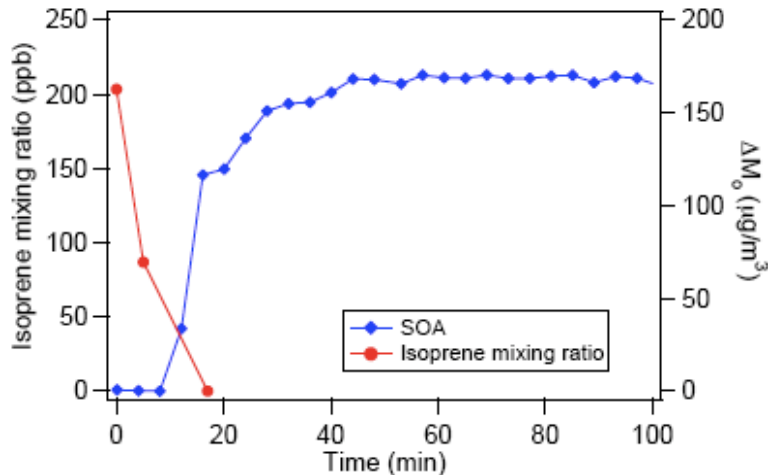


Figure 27. Total SOA along with the contributions from the various isoprene-related SOA lumps, linear scale on left, logarithmic scale on right, for the final simulation of the high- $\text{NO}_x$  scenario.

### Isoprene + $\text{NO}_3$

Here, an experiment reported by Ng et al. (2008) is simulated. The initial isoprene concentration was reported to be 0.2034 ppm at  $T = 294 \text{ K}$ . Dinitrogen pentoxide ( $\text{N}_2\text{O}_5$ ) provides the source for  $\text{NO}_3$  in the chamber. The GC measurements in the chamber were made every 12 minutes, so only for experiments where the initial isoprene exceeds 100 ppb can the isoprene decay be captured experimentally. Ng et al. (2008) estimate that the average concentration of  $\text{NO}_3$  in the experiment shown in Figure 28 is  $\sim 140 \text{ ppt}$ . An attempt to replicate the isoprene decay shown in Figure 28 was made. An initial concentration of  $\text{N}_2\text{O}_5$  of 1 ppm at 294 K reacted isoprene to zero in three minutes and resulted in a final concentration of  $\text{NO}_3$  of 850 ppt (Figure 29). The shape of the curve shown in Figure 28 was best reproduced from an initial value of  $\text{N}_2\text{O}_5$  of  $\sim 0.25 \text{ ppm}$  (Figure 29). This led to a final concentration of  $\text{NO}_3$  of 24 ppt and a much better approximation of the average value of  $\sim 140 \text{ ppt}$  reported by Ng et al. (2008).



**Fig. 2.** Reaction profile of the oxidation of an initial mixture containing 203.4 ppb isoprene ( $573 \mu\text{g}/\text{m}^3$ ).

Figure 28. Figure from Ng et al. (2008) showing rapid isoprene decay (red) followed by aerosol growth (blue).

Similar to, but far more dramatic than, the high- $\text{NO}_x$  case in which only one compound significantly contributed to the total mass (both in gas- and aerosol-phase), only the NV (UR6105) that forms from the  $\text{RO}_2+\text{RO}_2$  reaction following initial isoprene oxidation by  $\text{NO}_3$  in the dark plays any significant role here (Figure 30). The next contributor to the gas-phase is the MCR NV UR6302, and that exhibits a concentration that is 6 orders of magnitude smaller. The NV from OH related  $\text{RO}_2+\text{RO}_2$  reactions comes in third, with the epoxides contributing the least.

The model with all of these changes was applied to  $\text{NO}_3$  tests. That is, all four NV species have vapor pressures decreased by a factor of  $1\text{E}4$ , the epoxide NV represents 25% of the epoxide products, and the MCR NV represents 70% of the MCR+OH products (because the presence of  $\text{NO}_3$  can be considered as high- $\text{NO}_x$ ). As expected from the gas-phase results, the only contributor to SOA that matters is lump 20

(UR6105). These results capture the temporal behavior of the curve shown in Figure 28 quite well. Aerosol growth commences a bit sooner in the simulation, but the peak value is attained at approximately the same time ( $\sim 50$  min). However, the simulation fails to capture the magnitude of the aerosol mass by about an order of magnitude:  $\sim 160 \mu\text{g}/\text{m}^3$  in the laboratory versus  $17 \mu\text{g}/\text{m}^3$  in the simulation.

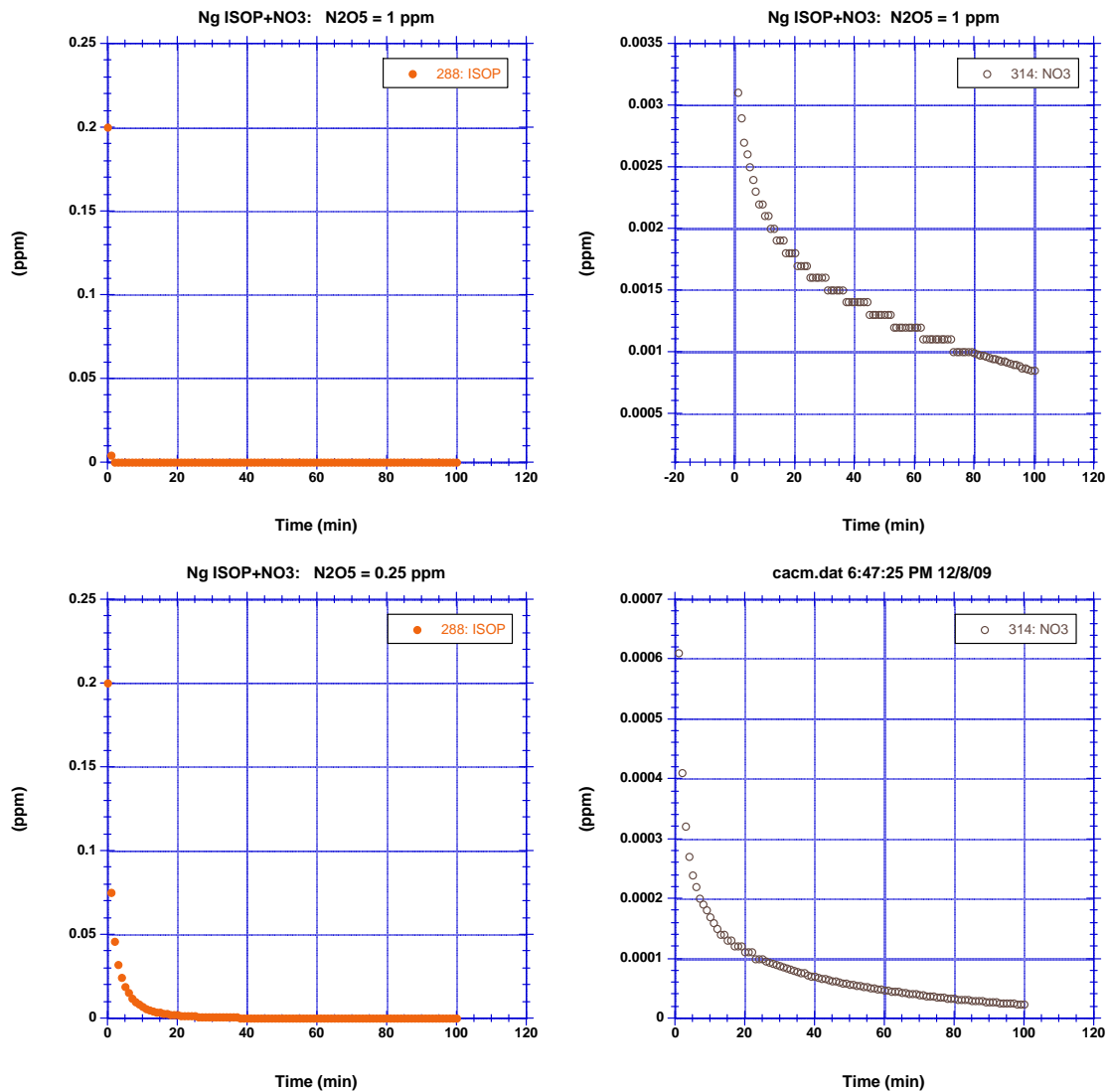


Figure 29. Comparison of isoprene (left panels) and NO<sub>3</sub> (right panels) for two initial values of [N<sub>2</sub>O<sub>5</sub>] = 1 ppm (top panels) and 0.25 ppm (bottom panels).

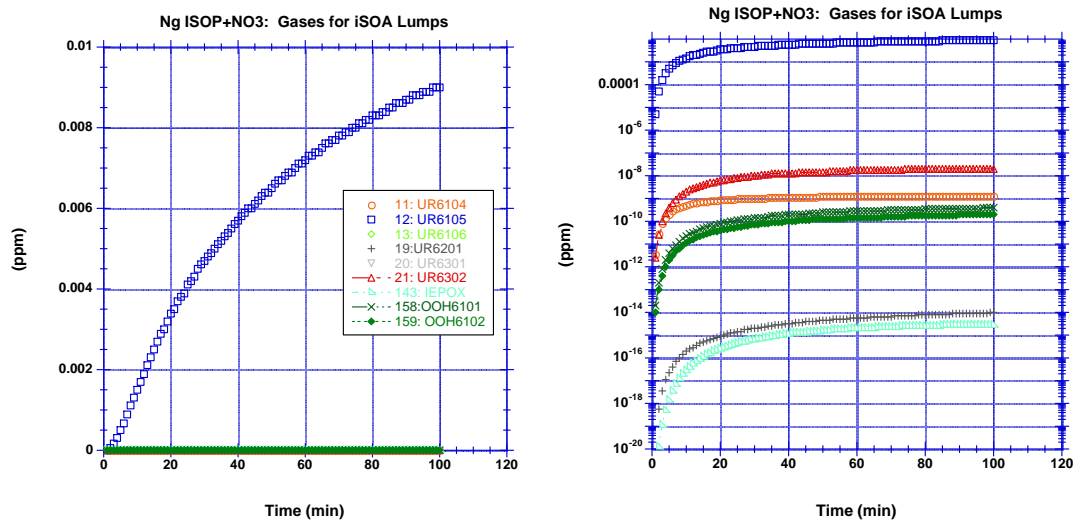


Figure 30. Gases relevant to SOA formation from isoprene with initial  $[N_2O_5] = 0.25$  ppm, linear scale on left, logarithmic scale on right.

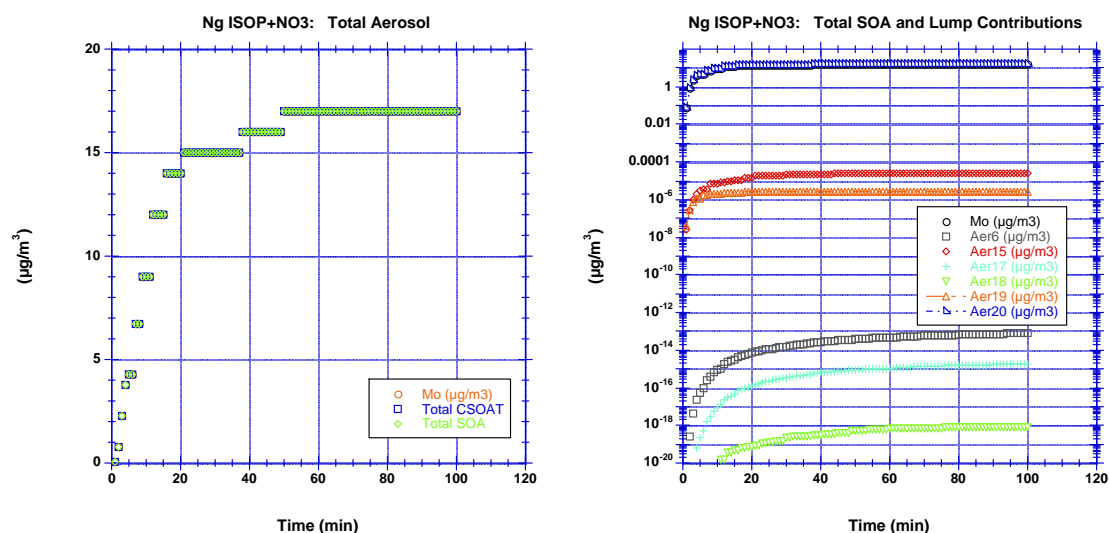


Figure 31. Total SOA and the contributions from the individual lumps as in Figure 30.

As in the high- $NO_x$  case, all NV (including UR6105) partition completely to the aerosol phase (as they should by definition). This is reflected in the total aerosol mass plot where all available mass (CSOAT) that can partition (blue squares, Figure 31) does so. Hence, to increase SOA mass requires producing more UR6105 in the gas phase.

It is possible that the choice of using  $[N_2O_5] = 0.25$  ppm was poor given the limited data shown in Figure 28. If  $[N_2O_5] = 0.5$  ppm, SOA mass increases to  $47 \mu\text{g}/\text{m}^3$ . If  $[N_2O_5]$  is further increased to 1.0 ppm, the SOA mass increases to  $63 \mu\text{g}/\text{m}^3$ , which is still less than half that observed in the chamber. Unlike the NV UR6302 and UR6106 where an initial arbitrary amount was chosen to go into these products (since they are essentially placeholders for unknown chemistry), the mechanism to form UR6105 was calculated more explicitly according to the chemical mechanism given in Ng et al. (2008). As a result, it is not a simple matter to arbitrarily increase the fraction formed without more detailed information to justify the change. Again, it is possible that a corresponding MCR NV from  $\text{NO}_3$  oxidation could be causing part of this underprediction.

This particular experiment was chosen as the test case because Figure 28 was useful in estimating the  $\text{N}_2\text{O}_5$  concentration required, given the discrepancy of the simulation depleting isoprene in three rather than 20 minutes. Other experiments were performed by Ng et al. (2008), and those results are summarized in Table 1. Neglecting the final two studies that were special cases, the yields range widely from 4.3% to 23.8%. In fact, the test case here is not listed in the table. Assuming a final SOA mass of  $160 \mu\text{g}/\text{m}^3$  (Figure 28) and  $0.2034$  ppm ( $566.65 \mu\text{g}/\text{m}^3$ ) of isoprene reacted, the estimated yield from Figure 28 is 28%, larger than any yield in Table 2. In contrast, the base simulation here produced  $17 \mu\text{g}/\text{m}^3$  for a yield of 3%. If the initial concentration of  $\text{N}_2\text{O}_5$  were too small in the simulation, the simulated yields could be 8% ( $47 \mu\text{g}/\text{m}^3$  for  $[N_2O_5] = 0.5$  ppm) or 11% ( $63 \mu\text{g}/\text{m}^3$  for  $[N_2O_5] = 1$  ppm). These represent the lower half of the values reported in Table 1.

**Table 1.** SOA yields from isoprene-NO<sub>3</sub> extracted from Ng et al. (2008).**Table 1.** Initial conditions and results for yield experiments.

Date	T (K)	RH (%)	$\Delta\text{HC}$ (ppb) <sup>a</sup>	$\Delta\text{M}_o$ ( $\mu\text{g}/\text{m}^3$ ) <sup>b</sup>	SOA Yield (%)
8/9/07	294	5.1	101.6 $\pm$ 0.6	68.1 $\pm$ 1.1	23.8 $\pm$ 0.5
8/10/07	293	4.7	30.2 $\pm$ 0.1	11.5 $\pm$ 0.4	13.5 $\pm$ 0.5
8/11/07	294	5.4	67.1 $\pm$ 0.1	39.3 $\pm$ 1.2	20.8 $\pm$ 0.7
8/12/07	293	6.0	51.7 $\pm$ 0.2	26.7 $\pm$ 0.6	18.2 $\pm$ 0.5
8/13/07	294	5.7	18.4 $\pm$ 0.1	2.2 $\pm$ 0.2	4.3 $\pm$ 0.5
8/14/07	294	5.5	21.8 $\pm$ 0.1	4.8 $\pm$ 0.4	7.8 $\pm$ 0.6
10/4/2007 <sup>c</sup>	293	5.5	39.5 $\pm$ 0.1 <sup>d</sup>	7.9 $\pm$ 0.3	7.1 $\pm$ 0.6
10/25/2007 <sup>e</sup>	294	6.4	42.0 $\pm$ 0.1	16.6 $\pm$ 0.6	14.1 $\pm$ 0.7

<sup>a</sup> Stated uncertainties ( $1\sigma$ ) are from scatter in isoprene measurements.

<sup>b</sup> Stated uncertainties ( $1\sigma$ ) are from scatter in particle volume measurements.

<sup>c</sup> Slow isoprene injection experiment.

<sup>d</sup> Concentration estimated based on a separate calibration experiment (see Sect. 3.2); the uncertainty in the measured isoprene concentration is assumed to be the same as in the slow N<sub>2</sub>O<sub>5</sub> injection experiment.

<sup>e</sup> Slow N<sub>2</sub>O<sub>5</sub> injection experiment.

Running a test for one of the smaller concentration cases in Table 1, the simulated yield was still too small. For the case where 0.0218 ppm of isoprene is consumed, the simulation produced 2.9  $\mu\text{g}/\text{m}^3$  of aerosol (4.8% yield) while Ng et al. (2008) observed 4.8  $\mu\text{g}/\text{m}^3$  with a 7.8% yield. In the simulation, using more N<sub>2</sub>O<sub>5</sub> did not help, presumably because 0.25 ppm was sufficient to consume the isoprene fully. Given the uncertainties of this chemical mechanism, it is difficult to know how to best change it to better capture the observations beyond hypothesizing SOA forming in a MCR-NO<sub>3</sub> reaction. Again, this reaction is being investigated as part of the process converting this report to a scientific manuscript.

### *MGLY and GLY*

The experimental studies considering uptake of MGLY and GLY to aerosol surfaces generally have focused on conversion of these gases to aerosol in the presence of

aqueous/acid particles. However, in the chamber simulations described above, no aqueous aerosol was present; therefore, this mechanism was not relevant for the simulation of SOA formation from isoprene via traditional gas-particle partitioning thermodynamics. However, in an effort to determine the possible relative importance of this mechanism compared to gas-particle partitioning, a simulation was performed, as discussed previously, in which GLY and MGLY were converted to NV species assuming first-order reaction rate constants of  $0.049 \text{ hr}^{-1}$  and  $0.073 \text{ hr}^{-1}$ , respectively. The masses of these NV species were simply added to the mass determined by traditional gas-particle partitioning. For the scenarios presented here, the summed amount of MGLY and GLY formed here is on the order of single digits of ppb based on the initial conditions and the stoichiometric factors used in CACM. Based on the rate constants used/assumed, about half of this material will lead to SOA formation, accounting for on order  $0.2 \mu\text{g}/\text{m}^3$  of additional SOA once appropriate unit conversions are incorporated. This is a small number for these simulations, but it should be stressed that the relative importance of this pathway depends strongly on the initial conditions chosen and the assumed first-order rate constants. Because this estimate makes this route seem less important than discussed in Fu et al. (2008), this code is being reviewed before its provision and before a scientific manuscript is submitted.

## **Conclusions**

Based on the modeling scenarios described above, several significant conclusions can be made regarding the simulation of SOA formation from isoprene:

- 1.) Despite a lack of understanding of the complex chemical mechanisms that lead to

the formation of the products that form SOA in this system, a relatively simple approach that leads to the formation of NV products works fairly well;

- 2.) For the simulation conditions chosen, traditional gas-particle partitioning theory (Raoult's Law) appears to be more important than does reactive uptake of the dicarbonyls GLY and MGLY;
- 3.) For the traditional approach, formation of low-volatility species (termed here as NV, likely to be dimers, trimers, etc.) is critical;
- 4.) The formation route of these NV species depends strongly on the conditions chosen;
- 5.) In photochemical scenarios in which abundant  $\text{NO}_x$  is present, oxidation of MCR by OH appears to have a critical role;
- 6.) In photochemical scenarios in which no  $\text{NO}_x$  is present, the oxidation of epoxides (which are formed from peroxides that only form when  $\text{NO}_x$  is absent) appears to have a critical role;
- 7.) In a nitrate radical scenario, organic peroxy radical self reactions are critical;
- 8.) It is possible that MCR- $\text{NO}_3$  reactions play an important role in both photochemical and dark systems; and
- 9.) Although some details of the gas-phase oxidation mechanism of isoprene remain unclear, this mechanism/approach can be updated as more information becomes available in the literature.

## References Cited

- Altieri, K.E., Carlton, A.G., Lim, H.J., Turpin, B.J., and Seitzinger, S.P., Evidence for oligomer formation in clouds: Reactions of isoprene oxidation products, *Environ. Sci. Technol.*, 40, 4956-4960, 2006.
- Carlton, A.G., Turpin, B.J., Lim, H.J., Altieri, K.E., and Seitzinger, S., Link between isoprene and secondary organic aerosol (SOA): Pyruvic acid oxidation yields low volatility organic acids in clouds, *Geophys. Res. Lett.*, 33, L06822, doi:10.1029/2005GL025374, 2006.
- Carlton, A.G., Wiedinmyer, C., and Kroll, J.H., A review of secondary organic aerosol (SOA) formation from isoprene, *Atmos. Chem. Phys.*, 9, 4987-5005, 2009.
- Chen, J., and Griffin, R.J., Modeling secondary organic aerosol formation from oxidation of  $\alpha$ -pinene,  $\beta$ -pinene, and d-limonene, *Atmos. Environ.*, 39, 7731-7744, 2005.
- Chen, J., Mao, H., Talbot, R.W., and Griffin, R.J., Application of the CACM and MPMPPO modules using the CMAQ model for the eastern United States, *J. Geophys. Res.*, 111, D23S25, doi:10.1029/2006JD007603, 2006.
- Claeys, M., et al., Formation of secondary organic aerosols through photooxidation of isoprene, *Science*, 303, 1173-1176, 2004.
- Fu, T.M., Jacob, D.J., Wittrock, F., Burrows, J.P., Vrekoussis, M., and Henze, D.K., Global budgets of atmospheric glyoxal and methylglyoxal, and implications for formation of secondary organic aerosols, *J. Geophys. Res.*, 113, D15303, doi:10.1029/2007JD009505, 2008.
- Goldstein, A.H., and Galbally, I.E., Known and unexplored organic constituents in the Earth's atmosphere, *Environ. Sci. Technol.*, 41, 1514-1521, 2007.
- Griffin, R.J., Dabdub, D., and Seinfeld, J.H., Development and initial evaluation of a dynamic species-resolved model for gas-phase chemistry and size-resolved gas/particle partitioning associated with secondary organic aerosol formation, *J. Geophys. Res.*, D05304, doi:10.1029/2004JD005219, 2005.
- Griffin, R.J., Dabdub, D., and Seinfeld, J.H., Secondary organic aerosol, 1. Atmospheric chemical mechanism for production of molecular constituents, *J. Geophys. Res.*, 107, 4332, doi: 10.1029/2001JD000541, 2002.
- Griffin, R. J., Nguyen, K., Dabdub, D., and Seinfeld, J.H., A coupled hydrophobic-hydrophilic model for predicting secondary organic aerosol formation, *J. Atmos. Chem.*, 44, 171-190, 2003.
- Guenther, A., et al., A global model of natural volatile organic compounds emissions, *J. Geophys. Res.*, 100, 8873-8892, 1995.

- Hallquist, M., et al., The formation, properties, and impact of secondary organic aerosol: current and emerging issues. *Atmos. Chem. Phys.*, 9, 5155-5235, 2009.
- Jenkin, M.E., Saunders, S.M., and Pilling, M.J., The tropospheric degradation of volatile organic compounds: a protocol for mechanism development, *Atmos. Environ.*, 31, 81-104, 1997.
- Jordan, C.E., Ziemann, P.J., Griffin, R.J., Lim, Y.B., Atkinson, R., and Arey, J., Computational simulation of the formation of secondary organic aerosol from oxidation of alkanes by the hydroxyl radical, *Atmos. Environ.*, 42, 8015-8026, 2008.
- Kroll, J.H., Ng, N.L., Murphy, S.M., Flagan, R.C., and Seinfeld, J.H., Secondary organic aerosol formation from isoprene photooxidation, *Environ. Sci. Technol.*, 40, 1869-1877, 2006.
- Kroll, J.H., Ng, N.L., Murphy, S.M., Flagan, R.C., and Seinfeld, J.H., Secondary organic aerosol formation from isoprene photooxidation under high-NO<sub>x</sub> conditions, *Geophys. Res. Lett.*, 32, L18808, doi:10.1029/2005GL023637, 2005a.
- Kroll, J.H., Ng, N.L., Murphy, S.M., Varutbangkul, V., Flagan, R.C., and Seinfeld, J.H., Chamber studies of secondary organic aerosol growth by reactive uptake of simple carbonyl compounds, *J. Geophys. Res.*, 110, D23207, doi:10.1029/2005JD006004, 2005b.
- Ng, N.L., et al., Secondary organic aerosol (SOA) formation from reaction of isoprene with nitrate radicals (NO<sub>3</sub>), *Atmos. Chem. Phys.*, 8, 4117-4140, 2008.
- Pandis, S.N., Paulson, S.E., Seinfeld, J.H., and Flagan, R.C., Aerosol formation in the photooxidation of isoprene and beta-pinene, *Atmos. Environ.*, 25, 997-1008, 1991.
- Paulot, F., Crounse, J.D., Kjaergaard, H.G., Kurten, A., St. Clair, J.M., Seinfeld, J.H., and Wennberg, P.O., Unexpected epoxide formation in the gas-phase photooxidation of isoprene, *Science*, 325, 730-733, 2009.
- Perring, A.E., Wisthaler, A., Graus, M., Wooldridge, P.J., Lockwood, A.L., Mielke, L.H., Shepson, P.B., Hansel, A., and Cohen, R.C., A product study of the isoprene + NO<sub>3</sub> reaction, *Atmos. Chem. Phys.*, 9, 4945-4956, 2009.
- Pun, B.K., Griffin, R.J., Seigneur, C., and Seinfeld, J.H., Secondary organic aerosol: II. Thermodynamic model for gas/particle partitioning of molecular constituents, *J. Geophys. Res.*, 107, 4333, doi: 10.1029/2001JD000542, 2002.
- Seinfeld, J.H., Erdakos, G.B., Asher, W.E., and Pankow, J.F., Modeling the formation of

- secondary organic aerosol (SOA) 2. The predicted effects of relative humidity on aerosol formation in the  $\alpha$ -pinene-,  $\beta$ -pinene-, sabinene-,  $\Delta^3$ -carene-, and cyclohexene-ozone systems, *Environ. Sci. Technol.*, 35, 1806–1817, 2001.
- Seinfeld, J.H., and Pandis, S.N., *Atmospheric Chemistry and Physics: From Air Pollution to Climate Change*, 2<sup>nd</sup> ed, Wiley-Interscience, 2006.
- Seinfeld, J.H., and Pankow, J.F., Organic atmospheric particulate matter, *Ann. Rev. Phys. Chem.*, 54, 121-140, 2003.
- Surratt, J.D., et al., Chemical composition of secondary organic aerosol formed from the photooxidation of isoprene, *J. Phys. Chem. A*, 110, 9665-9690, 2006.
- Volkamer, R., Jimenez, J.L., SanMartini, F., Dzepina, K., Zhang, Q., Salcedo, D., Molina, L.T., Worsnop, D.R., and Molina, M.J., Secondary organic aerosol formation from anthropogenic air pollution: Rapid and higher than expected, *Geophys. Res. Lett.*, 33, L17811, doi: 10.1029/2006GL026899, 2006.
- Wiedinmyer, C., Guenther, A., Estes, M., Strange, I.W., Yarwood, G., and Allen, D.T., A land use database and examples of biogenic isoprene emission estimates for the state of Texas, USA, *Atmos. Environ.*, 35, 6465-6477, 2001.
- Zhang, Q., et al., Ubiquity and dominance of oxygenated species in organic aerosols in anthropogenically-influenced Northern Hemisphere midlatitudes, *Geophys. Res. Lett.*, 34, L13801, doi:10.1029/2007GL029979, 2007.